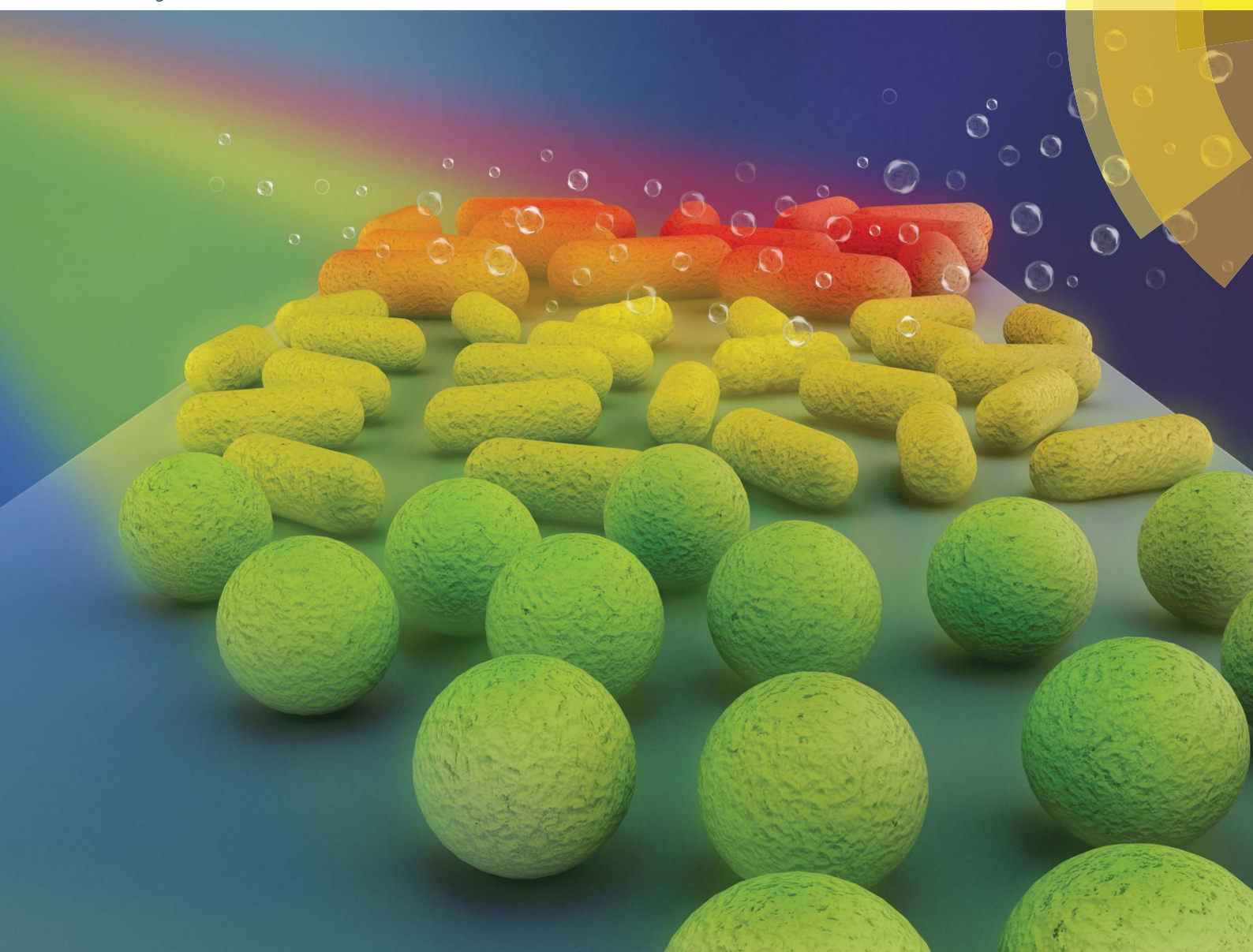
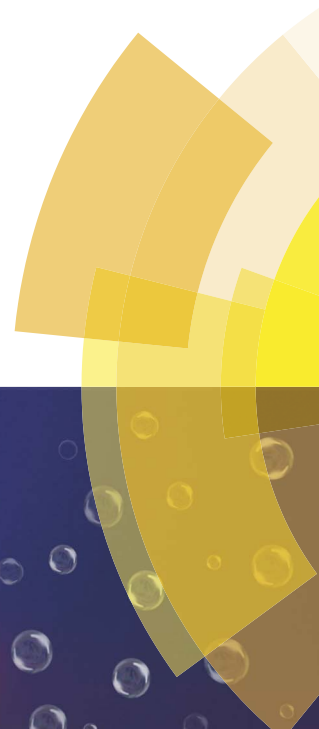


# Journal of Materials Chemistry A

Materials for energy and sustainability

[www.rsc.org/MaterialsA](http://www.rsc.org/MaterialsA)



ISSN 2050-7488



**REVIEW ARTICLE**

M. Valenti, W. A. Smith *et al.*

Plasmonic nanoparticle-semiconductor composites for efficient solar water splitting

**175** YEARS

CrossMark  
click for updatesCite this: *J. Mater. Chem. A*, 2016, 4, 17891

## Plasmonic nanoparticle-semiconductor composites for efficient solar water splitting

M. Valenti,<sup>\*a</sup> M. P. Jonsson,<sup>b</sup> G. Biskos,<sup>cd</sup> A. Schmidt-Ott<sup>a</sup> and W. A. Smith<sup>\*a</sup>

Photoelectrochemical (PEC) water splitting is a promising technology that uses light absorbing semiconductors to convert solar energy directly into a chemical fuel (*i.e.*, hydrogen). PEC water splitting has the potential to become a key technology in achieving a sustainable society, if high solar to fuel energy conversion efficiencies are obtained with earth abundant materials. This review article discusses recent developments and discoveries in the mechanisms by which the localized surface plasmon resonance (LSPR) in metallic nanoparticles can increase or complement a neighbouring semiconductor in light absorption for catalytic water splitting applications. These mechanisms can mitigate the intrinsic optical limitations of semiconductors (*e.g.*, metal oxides) for efficient solar water splitting. We identify four types of enhancement mechanisms in the recent literature: (i) light scattering, (ii) light concentration, (iii) hot electron injection (HEI), and (iv) plasmon-induced resonance energy transfer (PIRET). (i) Light scattering and (ii) light concentration are light trapping mechanisms that can increase the absorption of light with energies above the semiconductor optical band-edge. These two mechanisms are ideal to enhance the absorption of promising semiconductors with narrow bandgap energies that suffer from limited absorption coefficients and bulk charge recombination. On the other hand, (iii) HEI and the recently discovered (iv) PIRET are mechanisms that can enhance the absorption also below the semiconductor optical band-edge. Therefore, HEI and PIRET have the potential to extend

Received 27th July 2016  
Accepted 3rd October 2016

DOI: 10.1039/c6ta06405a

[www.rsc.org/MaterialsA](http://www.rsc.org/MaterialsA)

<sup>a</sup>Materials for Energy Conversion and Storage (MECS), Department of Chemical Engineering, Faculty of Applied Sciences, Delft University of Technology, Delft 2628-BL, The Netherlands. E-mail: m.valenti@tudelft.nl; w.smith@tudelft.nl

<sup>b</sup>Laboratory of Organic Electronics, Department of Science and Technology, Campus Norrköping, Linköping University, SE-60174 Norrköping, Sweden

<sup>c</sup>Faculty of Civil Engineering and Geosciences, Delft University of Technology, Delft 2628-CN, The Netherlands

<sup>d</sup>Energy Environment and Water Research Center, The Cyprus Institute, Nicosia 2121, Cyprus



Marco Valenti is a Ph.D. student supervised by Prof. Dr Andreas Schmidt-Ott at Delft University of Technology, The Netherlands. His research is focused on developing efficient materials for solar-to-fuel energy conversion. His main interests are twofold: (i) improving the optoelectronic properties of water splitting semiconductor photoelectrodes by plasmonic nanoparticle functionalization, and

(ii) studying the activity/selectivity in the electrochemical CO<sub>2</sub> reduction over noble metal alloy nanoparticles.



Dr Magnus Jonsson is an assistant professor at the Laboratory of Organic Electronics at Linköping University in Sweden. Before that he was a post-doctoral Wenner-Gren Fellow at the Kavli Institute of Nanoscience at Delft University of Technology, the Netherlands. Dr Jonsson's research explores nano-optical phenomena for energy harvesting and bio-applications. Related topics of

interest include optoelectronic paper and nanofabrication. Important contributions include plasmonic nanopores for single-molecule detection and nanoplasmonic biosensors. He is the recipient of several grants and awards, including an Ingvar Carlsson Award from the Swedish Foundation for Strategic Research and the Elsevier Biosensors and Bioelectronics Award 2010.



the light utilization to visible and near-infrared wavelengths of semiconductors with excellent electrochemical properties, but with large bandgap energies. New techniques and theories that have been developed to elucidate the above mentioned plasmonic mechanisms are presented and discussed for their application in metal oxide photoelectrodes. Finally, other plasmonic and non-plasmonic effects that do not increase the device absorption, but affect the electrochemical properties of the semiconductor (e.g., charge carrier transport) are also discussed, since a complete understanding of these phenomena is fundamental for the design of an efficient plasmonic NP-semiconductor water splitting device.

## 1. Introduction

Photoelectrochemical (PEC) water splitting offers a sustainable and clean way to store solar energy in the form of a chemical fuel, *i.e.* hydrogen. This process has benefited from over 40 years of research,<sup>1,2</sup> and many advances have been made with respect to the materials used today,<sup>3,4</sup> while our overall

understanding of the photo physical-chemical processes involved in the overall reaction has improved significantly. The main challenges that remain for PEC water splitting are finding materials that can simultaneously harvest solar irradiation, create and separate electronic charges (electrons and holes), and drive the water reduction and oxidation reactions. Furthermore, in order to bring this technology to a practical level, the entire process must be accomplished by inexpensive earth abundant materials that are stable in an electrochemical environment.

The most successful materials used to drive the solar water splitting reaction are semiconductor photoelectrodes, where metal oxides like TiO<sub>2</sub>,<sup>1</sup> WO<sub>3</sub>,<sup>5,6</sup> Fe<sub>2</sub>O<sub>3</sub>,<sup>7-9</sup> Cu<sub>2</sub>O,<sup>10,11</sup> and BiVO<sub>4</sub> (ref. 12–15) have received the most attention. These materials have been extensively studied and have emerged as promising candidates for practical applications as they are made from earth abundant materials that are generally stable in aqueous environments. However, metal oxide photoelectrodes often have less than ideal opto-electronic and catalytic properties, exhibited by low absorption coefficients, large band gap energies, short charge carrier diffusion lengths and life-times, and sluggish reaction kinetics at their surface.<sup>3</sup> Therefore, significant efforts have been devoted to functionalize metal oxide semiconductors photoelectrodes to improve their optical, electronic, and catalytic properties.<sup>16–18</sup>



*Dr George Biskos is an Associate Professor at the Cyprus Institute and at the Delft University of Technology. Previously he has been a faculty member at the University of the Aegean and a Research Associate at Harvard University. He holds a PhD in Engineering from Cambridge University, and an MSc in Environmental Engineering from Imperial College, UK. His research interests are in the*

*broader area of aerosol science and technology, ranging from instrumentation development for measuring airborne particles, to atmospheric aerosols and aerosol based nanotechnology.*



*Prof. Dr Andreas Schmidt-Ott received his Ph.D. from ETH Zurich, Switzerland. There, he worked at the Atmospheric Physics Department and later at the Solid State Physics Laboratory. He spent a term at the Chemical Engineering Department of the University of California, Los Angeles as a Visiting Assistant Professor before joining Duisburg University, Germany. Here, he was first*

*Assistant Professor at the Faculty of Electrical Engineering and then became professor in the Mechanical Engineering Department. Since 2001 he is a Professor of Particle Technology in the Materials for Energy Conversion and Storage section at Delft University of Technology, Netherlands. He received the Smoluchowski Award in 1989.*



*Dr Wilson A. Smith is an Associate Professor in the Department of Chemical Engineering at Delft University of Technology. He received his BSc (2005) and PhD (2010) in Physics before moving to the Universite Pierre et Marie Curie/Sorbonne in Paris, France to begin studying chemical engineering. Since 2012, he has lead a research group in Delft that focuses on fundamental processes related*

*to photo electrochemical water splitting, electrocatalytic water oxidation, and CO<sub>2</sub> reduction catalysis using inorganic nano-structured materials. His group uses many in situ electrochemical characterization tools to examine the electrode/electrolyte interface in these systems, with the aim to develop stable, selective, and efficient catalysts for the sustainable conversion and storage of renewable energy.*



One promising solution is to decorate semiconductors with plasmonic nanoparticles (NPs).<sup>19–21</sup> These metallic NPs can increase the absorption of thin film semiconductor photoelectrodes (with low absorption coefficients) by either confining or scattering the light into the semiconductor (*i.e.*, light trapping).<sup>20–22</sup> In addition, plasmonic NPs can absorb visible light with lower energies (*i.e.* higher wavelengths) than the semiconductor band gap and subsequently transfer the absorbed energy to the semiconductor in the form of “hot electrons” (electrons with energies higher than the metal Fermi level)<sup>23,24</sup> or in a dipole–dipole interaction,<sup>25</sup> effectively extending the semiconductor absorption range. At the same time, the plasmonic NPs can significantly improve the electronic<sup>26</sup> and catalytic<sup>27</sup> properties of semiconductors when the NPs are placed at the semiconductor–electrolyte interface. All these possibilities have resulted in the synthesis and photoelectrochemical testing of many different plasmonic NP/semiconductor composites, to elucidate the phenomena and exploit their use for solar driven water splitting.<sup>18,25,28–31</sup>

Recent reviews<sup>19,32,33</sup> on plasmonic photocatalysis have mainly focused on plasmonic mechanisms that enhance the semiconductor absorption. However, less emphasis has been given to plasmonic and non-plasmonic NP effects on the charge transport properties and energetics of the semiconductor. In this review, we discuss how plasmonic NP size, shape, and composition affect the optical properties, charge transport and energetics of semiconductor photoelectrodes for PEC water splitting. Particular emphasis is given to decoupling plasmon-induced and non-plasmon-induced effects that are generated by NP/semiconductor composites, in order to gain mechanistic insights into the structure–functionality relationship of these promising architectures to improve PEC water splitting.

## 2. Localized surface plasmon resonance

Light in the UV-visible wavelength range can induce collective oscillations of the valence electrons in noble metal NPs.<sup>34,35</sup> This phenomenon is known as localized surface plasmon resonance (LSPR). The oscillating electron cloud (called localized surface plasmon) exhibits a life-time on the order of femtoseconds that is limited by different radiative and non-radiative damping processes.<sup>36</sup> The population of surface plasmons that decays by radiative damping is converted into photons, whereas, the population that decays by non-radiative damping is converted into electron–hole pairs by interband and intraband excitations (*cf.* Fig. 1).<sup>36</sup>

### 2.1. Absorption and scattering cross sections

Metal NPs whose surface plasmons mainly decay through non-radiative processes are called light absorbing NPs, since the irradiating energy (*e.g.*, solar radiation) is absorbed by the NPs and subsequently transferred to their surroundings (*e.g.*, by releasing heat). For applications where non-radiative processes are desired, light absorbing NPs with a large absorption cross-section and a small scattering (radiative decay) cross-section are

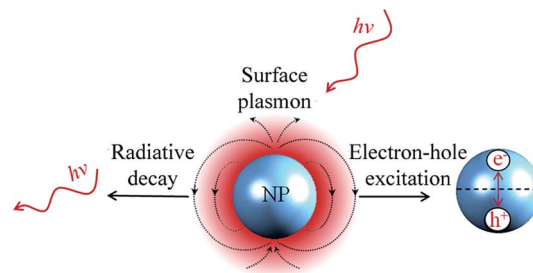


Fig. 1 Illustration of radiative (left) and non-radiative (right) decay of the NP surface plasmon. The non-radiative decay occurs due to intraband excitation within the conduction band.

selected. In 1908, Gustav Mie derived analytical expressions for the absorption and scattering cross-sections of spherical NPs of arbitrary size.<sup>34</sup> This theory has evolved to the generalized Mie theory that can also accurately predict the optical behaviour of particles of different shapes, such as ellipsoids and rods.<sup>37</sup> The NP scattering cross section ( $\sigma_{\text{sca}}$ ) and absorption cross section ( $\sigma_{\text{abs}}$ ) for small spheres can be approximated using eqn (1)–(3). This approximation is justified by Mie theory for spherical particles in the limit  $ak \ll 1$  and  $|mak| \ll 1$ , where  $a$  is the radius of the particle,  $k$  is the wave number and  $m$  is the refractive index of the particle relative to that of the medium.<sup>38</sup>

$$\sigma_{\text{abs}} = kIm(\alpha) \quad (1)$$

$$\sigma_{\text{sca}} = \frac{k^4}{6\pi} |\alpha|^2 \quad (2)$$

where  $\alpha$  is the particle polarizability, which for a small sphere can be expressed as:<sup>38</sup>

$$\alpha = 3V_p \frac{\epsilon - \epsilon_M}{\epsilon + 2\epsilon_M} \quad (3)$$

where  $V_p$  is the particle volume, and  $\epsilon$  and  $\epsilon_M$  are the wavelength dependent dielectric function of the NP material and surrounding medium, respectively. Resonant enhancement of the polarizability can hence occur for particles of materials with a negative real dielectric function (assuming a relatively small imaginary part). This illustrates why plasmonic excitations are found in metal nanoparticles.

For ellipsoidal NPs, a simple expression for the polarizability along direction  $i = 1, 2, 3$  can be obtained with the, less rigorous, electrostatic approximation (or dipole approximation) for small particles compared with the light wavelength:<sup>38</sup>

$$\alpha_i = V_p \frac{\epsilon - \epsilon_M}{\epsilon_M + L_i(\epsilon - \epsilon_M)} \quad (4)$$

where  $L_i$  are geometry factors along direction  $i = 1, 2, 3$  and whose sum should equal 1. For spheres,  $L_i = 1/3$ , which reproduce the expression in eqn (3) above.

Eqn (1)–(4) clearly show that the absorption and scattering cross sections depend on the NP size ( $V_p$ ), shape ( $L_i$ ) and composition ( $\epsilon$ ), along with the surrounding media ( $\epsilon_M$ ). Regarding size, the scattering cross section is proportional to  $V_p^2$ , while the absorption cross section is proportional to  $V_p$ . For example, Fig. 2 shows that the scattering cross section of



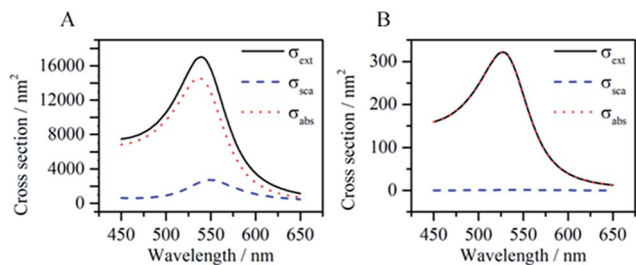


Fig. 2 Extinction, scattering and absorption spectra of a gold NP with a radius of 35 nm (A) and a radius of 10 nm (B) calculated using Mie theory. In both cases, the refractive index of the environment is 1.33.

a spherical gold NP nearly vanishes when its radius is decreased from 35 nm (Fig. 2A) to 10 nm (Fig. 2B), while the absorption cross section is decreased to a lesser extent. Therefore, small NPs are used for applications where only non-radiative decays are desired.

## 2.2. Plasmon resonance frequency

The light frequency at which the NP extinction coefficient is the greatest is called the NP plasmon resonance frequency, and it can be tuned by changing the material composition, shape and size of the NPs as shown in Fig. 3. Fig. 3A also highlights that noble metal NPs interact significantly with light that is abundant in the solar irradiation spectrum, which makes them excellent candidates to be used in solar energy conversion devices. The NP absorption and scattering spectra are also affected by the dielectric function of the surrounding medium (*cf.* eqn (1)–(3)). Even though the dielectric function of the surrounding medium is determined by the application (*e.g.*, aqueous solution for PEC water splitting), it can be partially modified by coating the NP with a thin semiconducting or insulating layer. The dielectric function and the thickness of the

coating can be changed to tune the resonance frequency of the NPs.<sup>39</sup>

Significant tunability of the LSPR extinction spectra has been achieved with metal NP rods and NP dimers (two closely spaced NPs), since they are characterized by two LSPR modes corresponding to excitation at different polarizations (*i.e.*, transversal and longitudinal modes).<sup>40–42</sup> In NP rods, the longitudinal mode can be accurately tuned by modifying the length of the rod,<sup>40</sup> whereas, for NP dimers the longitudinal mode can be tuned by modifying the interparticle distance (*cf.* Fig. 4).<sup>41,43</sup>

## 2.3. Light confinement (NP near-field)

An important characteristic of the LSPR is the highly localized electric field enhancement around the plasmonic NP. Fig. 5A shows the electric field contours of a silver NP when illuminated with light at the NP resonance frequency. It can be seen that the

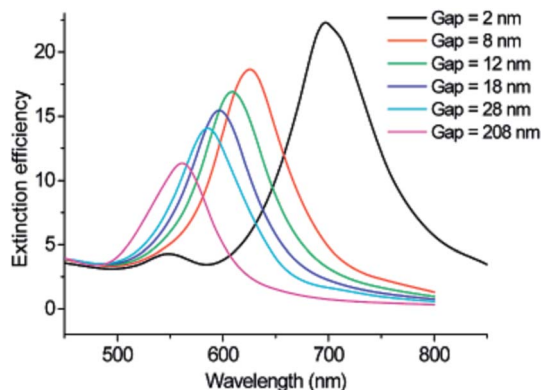


Fig. 4 Discrete dipole approximation-simulated extinction efficiency spectra of Au nanodisc pairs for varying interparticle separation gap for incident light polarized parallel to the interparticle axis (longitudinal mode). Reprinted with permission from ref. 43. Copyright 2007 ACS.

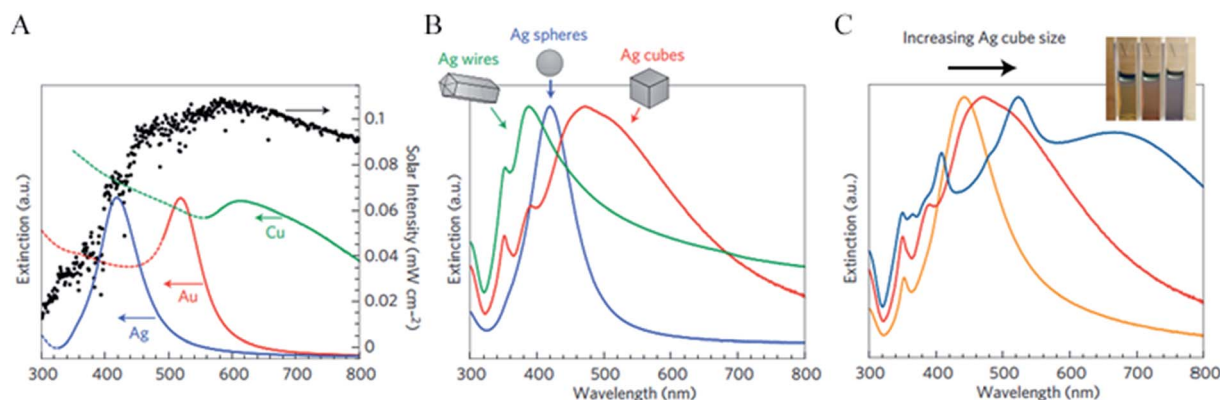


Fig. 3 (A) Normalized extinction spectra of spherical Ag ( $38 \pm 12$  nm in diameter), Au ( $25 \pm 5$  nm) and Cu ( $133 \pm 23$  nm) particles. The intensity of solar radiation (data for air mass 1.5 solar spectrum from the National Renewable Energy Laboratory, <http://rredc.nrel.gov/solar/spectra/am1.5/>) is also shown, in black. Dashed portions of the metal extinction curves indicate interband transitions (that is, no surface plasmon resonance in these regions). (B) Normalized extinction spectra for Ag wire, cube and sphere nanoparticles. Wire-shaped particles are  $90 \pm 12$  nm diameter and  $>30$  aspect ratio, cubic particles are  $79 \pm 12$  nm edge length and spherical particles are  $38 \pm 12$  nm diameter. (C) Normalized extinction spectra for Ag nanocubes as a function of size ( $56 \pm 8$  nm,  $79 \pm 13$  nm and  $129 \pm 7$  nm edge lengths correspond to orange, red and blue spectra respectively). The inset shows a photograph of the three nanocube samples suspended in ethanol.<sup>20</sup> Reprinted with permission from ref. 20. Copyright 2011 Macmillan publishers limited.



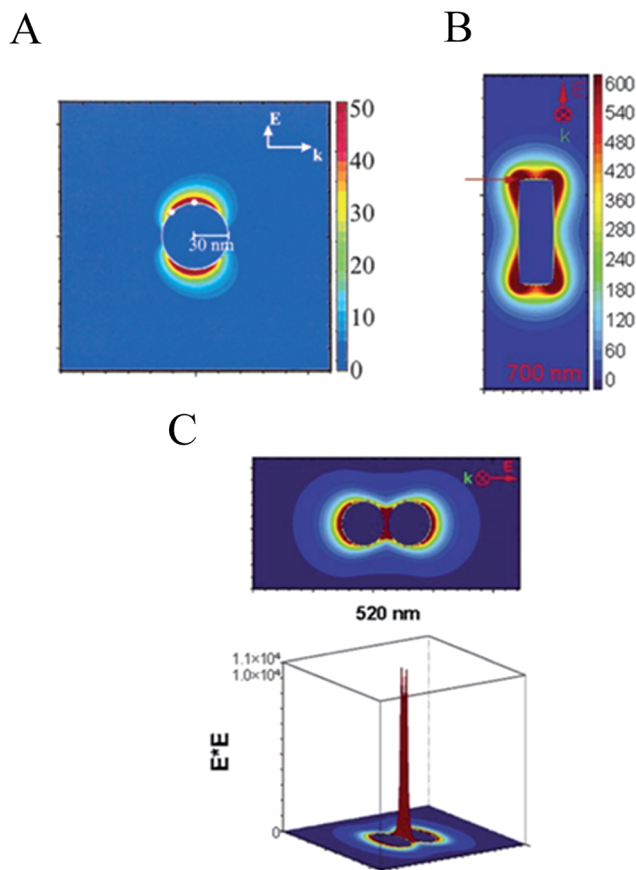


Fig. 5 (A) Electric field enhancement contours for a Ag sphere. Reprinted in part with permission from ref. 35. Copyright 2002 ACS (B) electric field enhancement contours for a rod. Reprinted in part with permission from ref. 47. Copyright 2004 AIP (C) electric field enhancement contours external to a dimer of Ag nanoparticles separated by 2 nm, for a plane that is along the inter-particle axis and that passes midway through the two particles. In the 3D plots, the axis perpendicular to the selected plane represents the amount of electric field enhancement around the dimer.<sup>47</sup> Reprinted in part with permission from ref. 47. Copyright 2004 AIP.

magnitude of the applied electric field is enhanced by  $\sim 50$  fold at the NP surface. This near-field effect plays an important role in several applications, such as waveguiding along particle chains,<sup>44</sup> surface-enhanced Raman scattering (SERS),<sup>45</sup> light trapping to enhance light absorption in semiconductors<sup>46</sup> (discussed in the following section), among others. Higher field enhancements are achieved with particles having sharp edges, such as the NP rod shown in Fig. 5B. Finally, the formation of NP dimers (e.g., spherical,<sup>47</sup> rod<sup>48</sup> and triangular prism<sup>47,49,50</sup> dimers) give rise to the largest field enhancements that are order of magnitudes larger than the applied field (cf. Fig. 5C).

### 3. Plasmonic NP/semiconductor composites

#### 3.1. Harvesting the surface plasmon's energy to drive the water splitting half reactions on semiconductors

For a NP in contact with a semiconductor, (part of) the surface plasmon's energy can be extracted for both radiative damping

and non-radiative damping (Fig. 6A and B). The surface plasmon energy can be transferred from the NP to the semiconductor and then further converted to chemical energy, for example, to drive the water splitting reactions. This energy transfer is possible through four different mechanisms that form the core of this review. These are (i) light scattering (radiative decay, Fig. 6A), (ii) hot electron injection (HEI, Fig. 6B), (iii) light concentration (Fig. 6C) and (iv) plasmon-induced resonance energy transfer (PIRET, Fig. 6D). Light scattering by radiative decay (i) can enhance the effective optical path length in the semiconductor. This leads to corresponding enhanced absorption and generation of charge carriers that can drive the water splitting half reactions (Fig. 6A).<sup>22</sup> Instead, when the surface plasmon decays by exciting an electron-hole pair within the NP (non-radiative decay, Fig. 6B) (ii), hot electrons can be transferred to the conduction band of the semiconductor. Once the hot electron and hole are separated, they can carry out the corresponding water splitting half reactions.<sup>23</sup> In the third (light concentration) and fourth (PIRET) mechanisms, the highly localized electric field enhancement (i.e., near-field) around the plasmonic NP induces interband excitations in a neighbouring semiconductor (Fig. 6C and D).<sup>51,52</sup> In both mechanisms, the plasmon energy transfer to the semiconductor is mediated by coupling between photons, plasmons and excitons (electron-hole pairs) in the NP near-field. Unlike direct light excitation, the near-field can induce excitations not only above, but also below the *optical band gap edge* (OBGE) of the semiconductor. This review distinguishes between near-field effects acting above the OBGE (i.e., light concentration mechanism) and below the OBGE (i.e., PIRET), since they have different implications (cf. Section 4.2.2). In the light concentration mechanism (iii) the NPs act as *optical antennas* that localize the incident electromagnetic field in the neighbouring semiconductor, increasing the electron-hole generation rate in the semiconductor (Fig. 6C).<sup>31,46,53</sup> In PIRET, the near-field energy is transferred *non-radiatively* to the semiconductor through strong dipole-dipole coupling with band edge states that are optically inaccessible (Fig. 6D).<sup>25</sup>

Because the light scattering (i) and the light concentration (iii) mechanisms both effectively guide and/or localize the incoming photons, these mechanisms are referred to as light trapping or photonic effects (Fig. 6A and C).<sup>54</sup> While the light trapping mechanisms are only effective with incident photon energies above the OBGE, HEI and PIRET can extend the light utilization to photon energies below the OBGE (Fig. 6B and D). These four energy transfer mechanisms (i.e., light scattering, HEI, light concentration and PIRET), allow decorating plasmonic NPs to enhance or complement the insufficient light absorption of bare semiconductors and, therefore, improve the overall performance of conventional water splitting semiconductor devices.

New strategies and materials have been developed in recent years to efficiently exploit the surface plasmon energy in plasmonic NP/metal oxide photoelectrodes in order to mitigate the optical limitations of bare semiconductor metal oxide photoelectrodes (i.e., large bandgap energies and low absorption coefficients).<sup>18,19,25-27,54-56</sup> Recent key publications that have



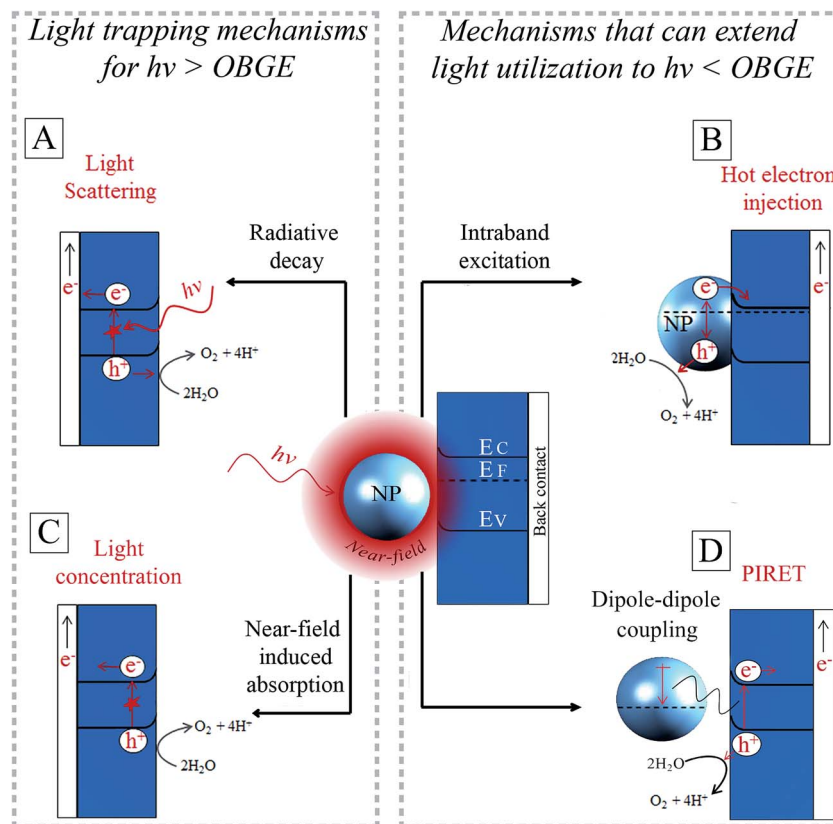


Fig. 6 Illustration of four energy transfer mechanisms from a plasmonic NP to an n-type semiconductor to drive water oxidation: (A) light scattering, (B) hot electron injection, (C) light concentration and (D) plasmon-induced resonance energy transfer (PIRET). OBGE denotes the optical band gap edge of the semiconductor.  $E_C$ ,  $E_F$ ,  $E_V$  are the conduction band, Fermi and valence band energies, respectively.

elucidated the roles of each mechanism for the water splitting performance of NP-metal oxide photoelectrodes are reviewed in Section 4 along with a more detailed description of the corresponding mechanisms.

### 3.2. Electrochemical effects

The plasmonic mechanisms described above are summarized in Fig. 7 together with other metal NP mechanisms, either plasmonic or non-plasmonic, that enhance the performance of semiconductor photoelectrodes. HEI, PIRET and light trapping are the mechanisms by which plasmonic NPs can increase the light absorption in the semiconductor. In addition, decorating plasmonic NPs on semiconductors can also cause other important electrochemical effects that can enhance the water splitting performance of the semiconductor. In turn, these electrochemical effects can be divided into those that affect (i) the semiconductor's charge transport, and (ii) its electronic band energetics (*cf.* Fig. 7). A significant challenge in plasmonic water splitting research has been to differentiate these two electrochemical effects from the plasmonic mechanisms that can increase the device absorption.<sup>22,27,28,55</sup> Several optical, electrochemical, and computational techniques have been successfully used to distinctly recognize the role of each effect in the water splitting process.<sup>18,22,27</sup> Consequently, while this review's main focus is to discuss the recent advances that

elucidate the potential of light trapping, HEI and PIRET to enhance the absorption of metal oxide semiconductors, a concluding section (Section 5) is dedicated to discuss other plasmonic and non-plasmonic effects (*cf.* Fig. 7) that also play an important role in improving the overall performance of the metal NP/semiconductor composite for solar water splitting devices.

## 4. Plasmonic energy transfer mechanisms

### 4.1. Hot electron injection (HEI)

Hot electrons are generated through non-radiative damping and hot electron injection (HEI) is therefore best exploited by light absorbing NPs. Fig. 8 shows a more detailed illustration of this mechanism. When the surface plasmons decay through intraband excitations within the conduction band, the excited electrons (hot electrons) obtain energies higher than the metal Fermi energy ( $E_F$ ; *cf.* Fig. 8).<sup>60,61</sup> For plasmonic NPs smaller than 20 nm the hot electron exhibit energies ( $E_H$ ) within the range  $E_F < E_H < E_F + \hbar\omega$ , while larger particles exhibit much smaller hot electron energies close to  $E_F$ .<sup>62</sup> If the energy of the hot electrons are larger than the interface Schottky energy barrier, the hot electrons can be transferred to the conduction band of the semiconductor.<sup>23,51,61,63-67</sup> Charge neutrality in the metal NP is



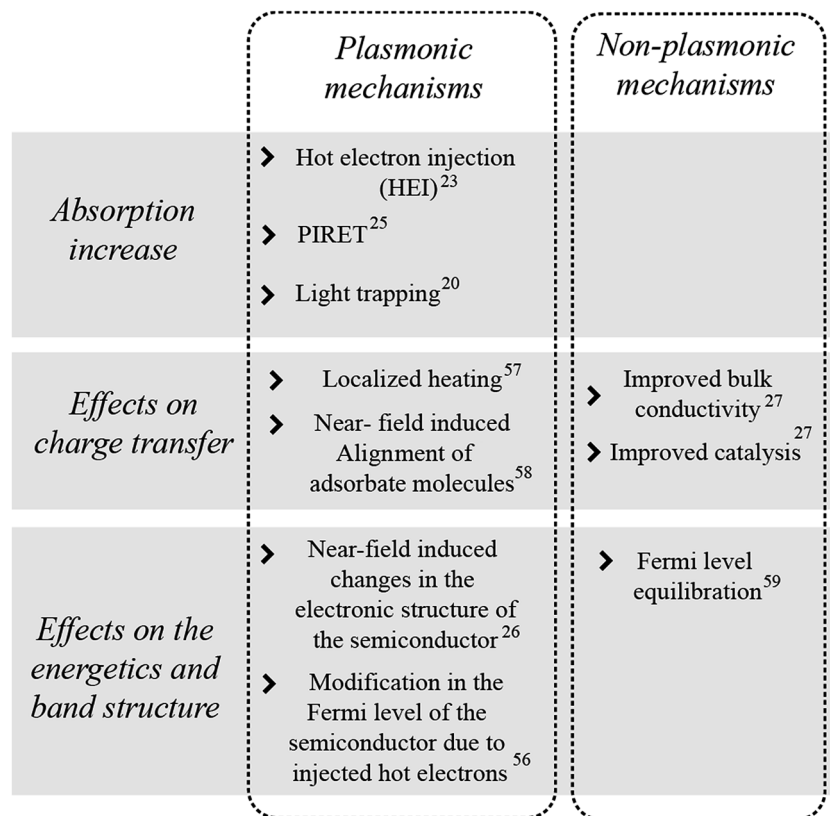


Fig. 7 Summary of proposed effects of metal NPs on semiconductors for photoelectrochemical water splitting.<sup>20,23,25–27,56–59</sup>

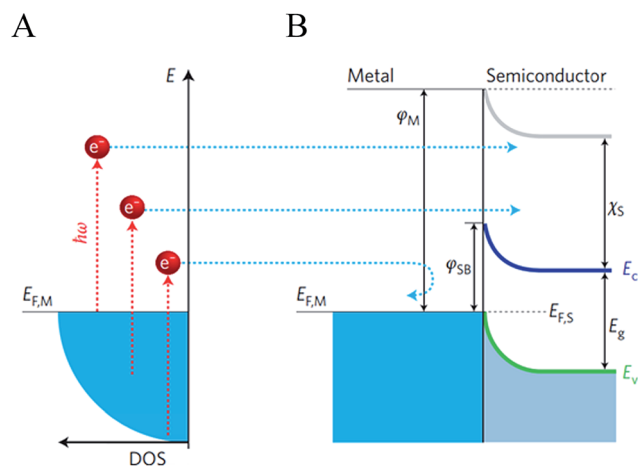


Fig. 8 (A) Plasmonic energy conversion: electrons from occupied energy levels are excited above the Fermi energy. (B) Hot electrons can be injected into a semiconductor by forming a Schottky barrier with the plasmonic nanostructure. Hot electrons with energies high enough to overcome the Schottky barrier  $\phi_{SB} = \phi_M - \chi_S$  are injected into the conduction band  $E_C$  of the neighbouring semiconductor, where  $\phi_M$  is the work function of the metal and  $\chi_S$  is the electron affinity of the semiconductor. Reprinted in part with permission from ref. 24. Copyright 2014 Macmillan publishers limited.

restored by removing the “hot hole” with an oxygen evolution catalyst (OEC) or an electron-donor solution (in the case of an n-type semiconductor). Excited electrons with energies lower than the Schottky barrier relax through, for instance, electron-

electron and electron-phonon collisions (releasing heat).<sup>68</sup> Therefore, the efficiency of the HEI mechanism is expected to decrease with increasing Schottky barrier energies, which depend on the energetics of the selected metal/semiconductor system. However, having energies larger than the Schottky barrier is by no means the only requirement for a hot electron to be injected to the conduction band of the semiconductor. The hot electron also needs to reach the surface of the NP, before undergoing another relaxation process.<sup>24</sup> Further limitations come from the non-ideal electron-acceptor ability of the semiconductor (*i.e.*, limited density of states in the conduction band) and the non-ideal electron-donor ability of the OEC/electrolyte that replaces the injected hot electrons.<sup>24,69–71</sup> The above limitations significantly affect the efficiency of HEI and it is of great importance to theoretically and experimentally study each limitation individually. One of the main challenges to experimentally study the HEI efficiency comes from the fact that the measured hydrogen/oxygen evolution in a plasmonic NP/semiconductor photoelectrode not only come from the HEI process (due to the NP light absorption) but also from light absorption of the semiconductor itself. Therefore, strategies must be developed to accurately decouple these two contributions before attempting the optimization of HEI. Two recent publications made key contributions to tackle this issue using two different approaches. Mubeen *et al.*,<sup>23</sup> fabricated a Au nanorod/TiO<sub>2</sub> composite system, where the TiO<sub>2</sub> layer was so thin that its only role was to remove the hot electrons from the nanorod (electron filter) and did not contribute to the measured



photocurrent. Chen *et al.*<sup>26</sup> used a different strategy based on a Au NP/ZnO composite and tested its photoelectrochemical ability to split water by illuminating it only with visible light that has lower energies than the ZnO band gap. That ensured that only photocurrent related to the HEI mechanism was measured. We start by reviewing the work by Mubeen *et al.* in detail in order to gain further insights to the HEI mechanism.

Mubeen *et al.* fabricated an autonomous plasmonic solar water splitting device where the oxygen and hydrogen evolution reaction take place on the NP-semiconductor composite without the use of external wires and without applying a bias voltage. This device consists of an array of vertically aligned gold nanorods in an aluminium oxide template. Fig. 9A and B, show an illustration and a transmission electron microscope (TEM) image of one of the nanorods, respectively. The plasmonic rod is capped with a thin layer of crystalline TiO<sub>2</sub>, which in turn is decorated with a hydrogen evolution catalyst (Pt NPs). On the side of the nanorod a cobalt-based oxygen evolution catalyst is deposited. In this device, all the charge carriers are derived from surface plasmons (through HEI) and the semiconductor works only as a hot electron filter as depicted in Fig. 9C. Using this approach, once the hot electrons and holes are separated, they migrate to the corresponding catalysts to carry out the water splitting half reactions. The autonomous device was operated with a 1 M potassium borate electrolyte (pH 9.6) under visible light illumination ( $\lambda > 410$  nm), exhibiting an external quantum efficiency (EQE) of  $\sim 0.1\%$  (averaged over the visible portion of the solar spectrum). Several strategies were taken in this work to confirm that all the charges indeed came from the HEI mechanism and not from conventional TiO<sub>2</sub> light absorption. One of them is shown in Fig. 10, where the hydrogen production of the device was measured under illumination with light of different spectral ranges. Under UV-dominated illumination ( $310 \text{ nm} < \lambda < 520 \text{ nm}$ ), the hydrogen production rate is much lower than

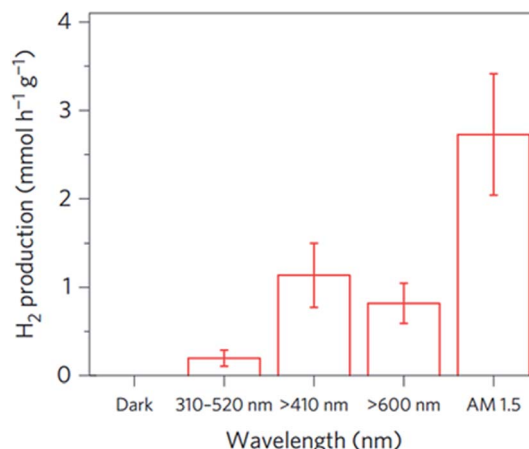


Fig. 10 Hydrogen produced per hour with various illumination wavelengths, each determined from an experiment in which the device was continuously illuminated for 9 h. Reprinted with permission from ref. 23. Copyright 2013 Macmillan publishers limited.

when the device is illuminated with visible light ( $\lambda > 410$  nm or  $\lambda > 600$  nm). The low performance under UV illumination confirms that conventional electron-hole excitation due to light absorption in the TiO<sub>2</sub> does not contribute to the hydrogen generation under AM 1.5 irradiation, since TiO<sub>2</sub> only absorbs light up to  $\sim 380$  nm. Therefore, this device is ideal to independently study the different processes that limit the HEI efficiency (*e.g.*, electron-donor ability of the hydrogen evolution catalyst). Finally, this work reports no decrease in activity over 66 hours of solar irradiation. This excellent stability represents a great advantage for plasmon driven water splitting devices when compared with conventional short bandgap metal oxide semiconductors that decrease their performance over time due to corrosion.<sup>72,73</sup>

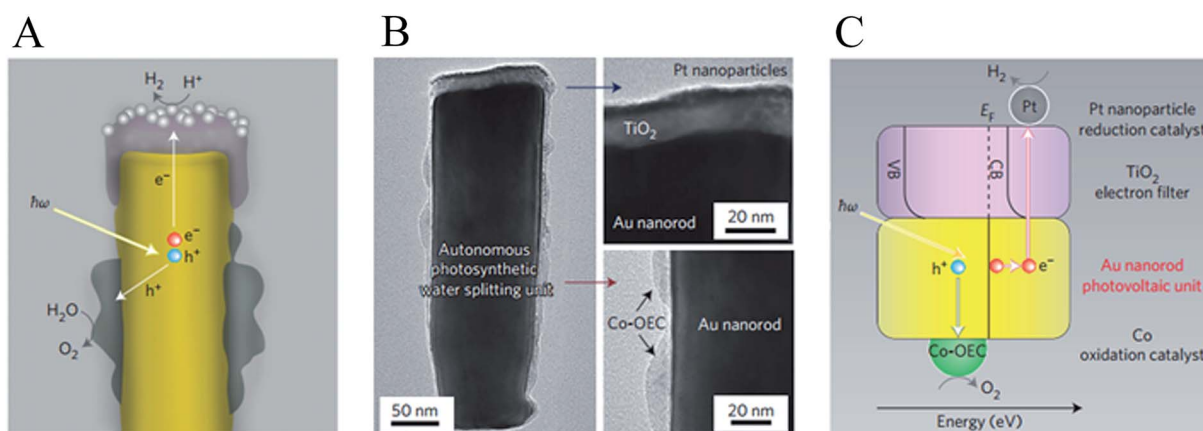


Fig. 9 Structure and mechanism of operation of the autonomous plasmonic solar water splitter. (A) Schematic of the cross-section of an individual photosynthetic unit showing the inner gold nanorod, the TiO<sub>2</sub> cap decorated with platinum nanoparticles, which functions as the hydrogen evolution catalyst, and the Co-OEC material deposited on the lower portion of the gold nanorod. (B) Corresponding transmission electron micrograph (left) and magnified views of the platinum/TiO<sub>2</sub> cap (top right) and the Co-OEC (bottom right). (C) Energy level diagram superimposed on a schematic of an individual unit of the plasmonic solar water splitter, showing the proposed processes occurring in its various parts and in energy space. CB, conduction band; VB, valence band; EF, Fermi energy. Reprinted with permission from ref. 23. Copyright 2013 Macmillan publishers limited.



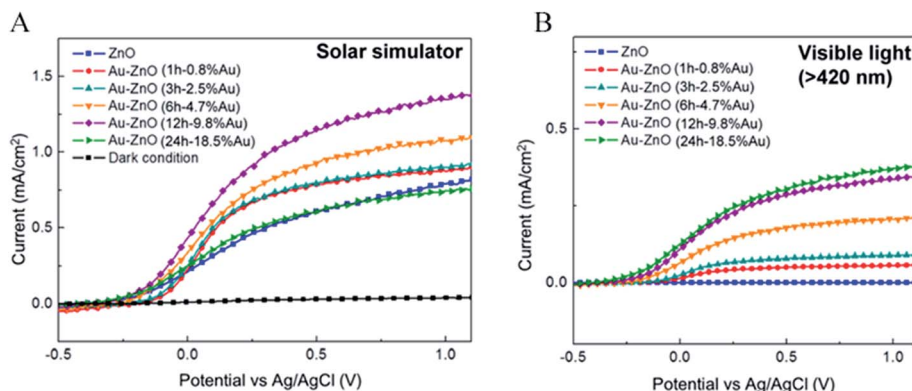


Fig. 11 (A) Linear-sweep voltammograms of Au–ZnO photoelectrodes with nanoparticles deposited for various periods, and a dark scan, performed in a 0.5 M aqueous  $\text{Na}_2\text{SO}_4$  with a pH of 6.8 under an AM 1.5 solar simulator. (B) Linear-sweep voltammograms of Au ZnO photoelectrodes with nanoparticles deposited for various periods, obtained under illumination by visible light (>420 nm). Reprinted with permission from ref. 26. Copyright 2012 ACS.

More recently, the same authors reported<sup>74</sup> photo-production of hydrogen with a similar system for gold nanorods with different aspect ratios, exhibiting longitudinal absorption modes nearly throughout the solar spectrum ( $\lambda \sim 400\text{--}1000$  nm). In this work, instead of an electron donor oxygen evolution catalyst, methanol was added to the electrolyte as a sacrificial reactant. The authors show that by using nanorods with different aspect ratios the hydrogen production can be doubled compared with a device that uses nanorods of the same dimensions. The device presented a EQE of  $\sim 0.1\%$  (averaged over the entire solar spectrum) and showed good stability for over 200 hours of continuous operation.

Unlike in the previously described works, Chen *et al.*<sup>26</sup> synthesized a NP/semiconductor composite where the semiconductor absorption contributes significantly to the composite's hydrogen generation. The NP/semiconductor composites used in this work consist of arrays of ZnO nanorods decorated with spherical gold NPs with an average size of less than 5 nm. These composites were used as the working electrode in a three electrode-based photoelectrochemical system, and cyclic voltammetry measurements under AM 1.5 solar simulation irradiation are shown in Fig. 11A. It is clear that the performance of the composite device increases with an increase in the plasmonic NP concentration, until an optimum NP loading of 9.8%. Fig. 11B, shows a similar type of experiment, but this time the sample was irradiated only with visible light (>420 nm). This visible light has lower energies than the semiconductor band gap and, as expected, no photocurrent was obtained in the cyclic voltammetry of the bare ZnO sample (*cf.* Fig. 11B). After NP deposition the photocurrent increased up to  $\sim 0.3 \mu\text{A cm}^{-2}$  at 1 V vs. Ag/AgCl, which the authors attribute to the HEI mechanism. In order to further elucidate the HEI effect, wavelength dependent photocurrent measurements were performed and compared with the NP absorption spectra. Fig. 12 shows that the measured photocurrent presents a peak around 2.4 eV, which corresponds well to the NP plasmon absorption mode. This correlation between the photocurrent and the absorption spectra gives further evidence that the obtained photocurrent is due to a plasmonic effect. This type of comparison is now

commonly used to prove plasmonic effects and has become an important tool in the plasmon driven water splitting field. However, it should be pointed out that hot electrons with sufficient energy to overcome the Schottky barrier may be excited also without plasmonic effects, *via* the photoelectric effect. Chen *et al.* also compared the measured photocurrent with the number of photoelectrons that derive from direct light excitation (photoelectric effect) and have sufficient energy to overcome the Schottky energy barrier. These photoelectrons (Fowler hot electrons) are calculated according to Fowler theory:

$$\eta_i = C_f \frac{(h\nu - \phi)^2}{h\nu} \quad (5)$$

where  $C_f$  is the Fowler emission coefficient and  $\phi$  is the Schottky energy barrier. Eqn (5) was fitted to the obtained photocurrent,

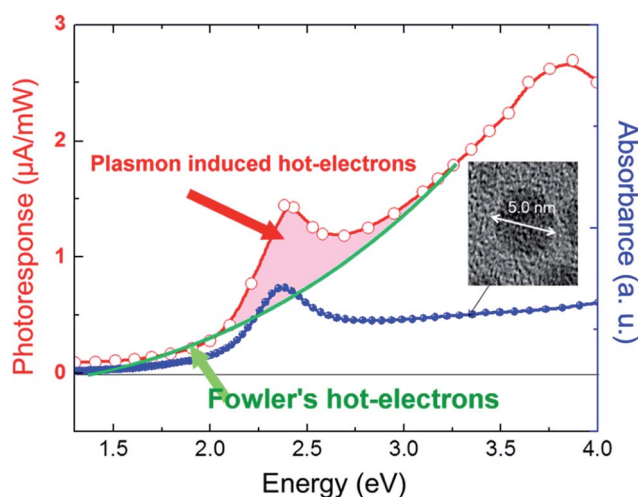


Fig. 12 Absorption spectrum of Au nanospheres and plots of photocurrent versus wavelength, fitted to Fowler's law, indicating that photocurrent comprises mainly hot electron flow, with additional contribution from hot electrons that are injected from Au under plasmonic-induced irradiation that is amplified by localized surface plasmon resonance. Reprinted with permission from ref. 26. Copyright 2012 ACS.



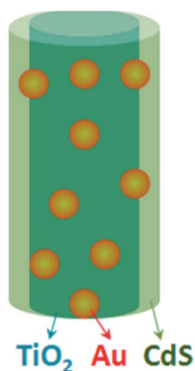


Fig. 13 Illustration of the sandwich CdS–Au–TiO<sub>2</sub> composite. Reprinted with permission from ref. 18. Copyright 2014 ACS.

as shown in Fig. 12. It can be clearly seen that the photocurrent diverges from the Fowler's relation around the NP resonance frequency, confirming that the hot electrons, associated with the surface plasmon resonance effect, significantly contribute to the composite's measured photocurrent (*cf.* Fig. 11A and B).

**4.1.1. Transient absorption analysis.** A more complex plasmonic composite, containing three light absorbing components, was synthesized by Li *et al.*<sup>18</sup> They used a CdS–Au–TiO<sub>2</sub> sandwich nanorod array as the photoanode in a water splitting PEC cell and studied the role of the plasmonic gold NPs on the composite's performance. The sandwich composite consists of a gold-decorated TiO<sub>2</sub> nanorod with an external

coating of CdS quantum dots (QDs), as illustrated in Fig. 13. The CdS QDs, like the plasmonic NPs, can be used as photosensitizers to extend the light absorption range of large band gap semiconductors.<sup>75–77</sup> Therefore, in this composite a large fraction of the solar spectrum is absorbed. TiO<sub>2</sub> absorbs light with wavelengths below  $\sim 400$  nm, CdS QDs below  $\sim 525$  nm and the plasmonic NPs below  $\sim 725$  nm. Fig. 14A shows the incident photon to current efficiency (IPCE) of the composite, with and without the gold NPs. It can be seen that the IPCE is slightly increased in the region of the spectrum around 650 nm, which corresponds to the location of the LSPR mode of the gold NPs. Moreover, at this wavelength neither of the semiconductor components (*i.e.*, TiO<sub>2</sub> and CdS QDs) absorb light, which indicates that the photocurrent may be due to the HEI mechanism in the plasmonic NPs. The authors used transient absorption analysis to elucidate the origin of this photocurrent increase. Fig. 14B shows the transient absorption signal (bottom of the figure) that corresponds to the TiO<sub>2</sub> trap state absorptions in the visible region. As expected, under 400 nm illumination for bare TiO<sub>2</sub> it can be clearly seen the filling of the TiO<sub>2</sub> trap states by the photogenerated charge carriers (blue line in Fig. 14B). What is more interesting is that under 675 nm illumination, filling of the TiO<sub>2</sub> trap states is also observed in the Au–TiO<sub>2</sub> and CdS–Au–TiO<sub>2</sub> composites (green and orange lines in Fig. 14B, respectively). Since neither of the semiconductors absorb 675 nm light, the filling of the TiO<sub>2</sub> trap states must be due to hot electron transfer from the plasmonic NP. Fig. 14B (top of the figure) also shows the blue-shift in the gold NP LSPR mode of

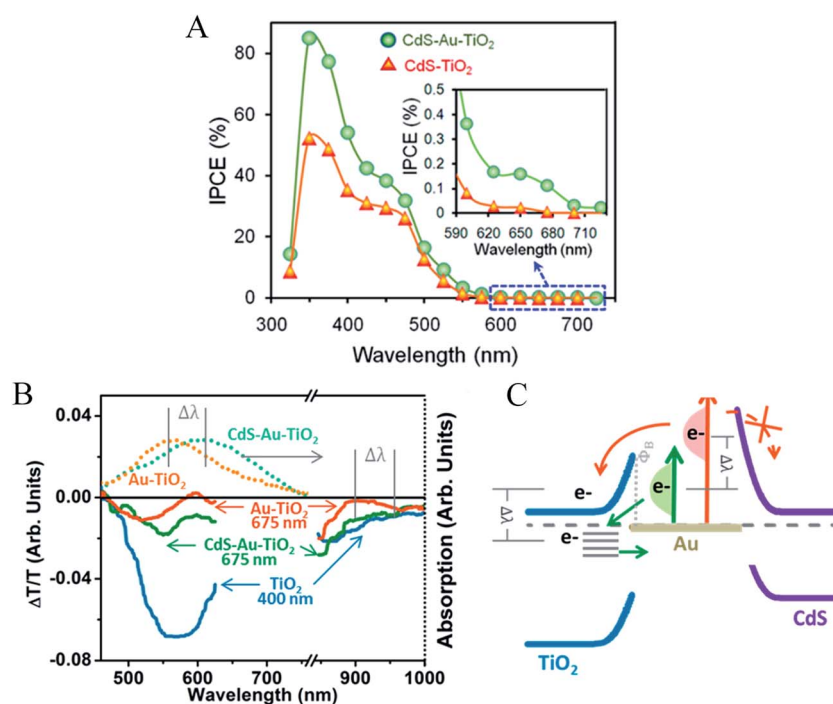


Fig. 14 (A) IPCE. (B) NP absorption in Au–TiO<sub>2</sub> and in CdS–Au–TiO<sub>2</sub> (Top) and full-spectrum transient absorption signal at 20 ps after excitation (bottom). (C) The change in back-transfer dynamics and filling of the TiO<sub>2</sub> electron-trap states without charge transfer into CdS is explained by the energy of the hot plasmonic electron distribution relative to the interfacial Schottky barrier. Reprinted with permission from ref. 18. Copyright 2014 ACS.



Au-TiO<sub>2</sub> compared with CdS-Au-TiO<sub>2</sub>. From the location in the spectrum of the LSPR and the transient absorption signal (Fig. 14B), the authors were able to shed light on the dynamics of the hot electron in the composites (*i.e.*, CdS-Au-TiO<sub>2</sub> and Au-TiO<sub>2</sub>) upon illumination with light at 675 nm (*cf.* Fig. 14C). A key observation is that the filling of the TiO<sub>2</sub> trap states is more efficient in CdS-Au-TiO<sub>2</sub> than for Au-TiO<sub>2</sub> (green and orange lines in Fig. 14B). This is consistent with the fact that, in comparison with Au-TiO<sub>2</sub>, the hot electrons in CdS-Au-TiO<sub>2</sub> have a lower energy (red-shifted LSPR). As a result the hot electrons are not able overcome the Schottky energy barrier, and are efficiently transferred to the TiO<sub>2</sub> trap states (green arrows in Fig. 14C). On the other hand, the hot electrons in Au-TiO<sub>2</sub> (with blue-shifted LSPR) exhibit a higher offset energy from the gold Fermi level and can overcome the Schottky energy barrier, reaching the TiO<sub>2</sub> conduction band (orange arrows in Fig. 14C). Therefore, by looking at the filling of TiO<sub>2</sub> trap states the authors were able to study the HEI efficiency of the synthesized plasmonic composites, which makes transient absorption analysis a very powerful tool to study the HEI in complex systems.

#### 4.1.2. Other design parameters for HEI devices

**4.1.2.1. NP composition.** As discussed above, the HEI efficiency highly depends on the hot electron energy. Hot electrons can be generated either by intraband or interband transitions. Recent theoretical studies<sup>78–81</sup> have shown that interband transitions induced by visible light (from the d-band) result in high energy hot holes but low energy hot electrons ( $\sim E_F$ ), due to the position of the d-band relative to the Fermi level in noble metals. By contrast, hot electrons generated by intraband transitions can have energies up to  $E_F + \hbar\omega$ .<sup>62</sup> Therefore, it is advantageous to use materials with a relatively large interband energy threshold to maximize the intraband excitation spectrum. Ag exhibits an interband energy of  $\sim 3.7$  eV and, therefore, only intraband transitions are expected when illuminated with visible light. Au on the other hand, has an interband energy of  $\sim 2.3$  eV and its HEI efficiencies may be limited by interband excitations when illuminated with violet, blue and green light.

The above reasoning holds for HEI over the Schottky energy barrier (as illustrated in Fig. 8), where the HEI efficiency depends on the hot electron energy. However, it has been recently proposed that low energy hot electrons (generated by interband transitions) can also be transferred to the semiconductor by tunnelling through the Schottky energy barrier.<sup>82</sup> Further research must be undertaken to study the efficiency of this hot electron transfer process.

The material composition of the NP is of great importance in the design of HEI water splitting devices, because it affects three important HEI parameters: (i) LSPR frequency, (ii) Fermi level equilibration, and (iii) the energy of the resulting charge carriers. Even though materials other than Au and Ag have been used for HEI applications, including Pt<sup>83,84</sup> and Al,<sup>30</sup> we believe that alloy NPs are particularly promising for future HEI devices. The use of alloy NPs allows for fine-tuning of these three important parameters to fit the requirements of specific hot electron acceptor semiconductor for specific applications.

**4.1.2.2. NP size.** NPs of less than 20 nm are used as hot electron injectors, since their hot electrons exhibit high energies (up to  $E_F + \hbar\omega$ ),<sup>62</sup> and can readily reach the NP surface where they are extracted. Since hot charge carriers created by intraband transitions have a mean free path of  $\sim 10$ – $40$  nm,<sup>78</sup> most of the generated hot carriers in these NPs ( $< 20$  nm) are expected to reach the surface before thermalization. In contrast, hot carriers created by interband excitations are expected to have much shorter mean free paths ( $\sim 1$  nm)<sup>78</sup> and, therefore, even smaller NPs (2–3 nm) are required for charge extraction. Particles smaller than 2 nm in size are called metal clusters, and exhibit a discrete molecule-like band structure. It has been reported that Au clusters with distinct highest occupied molecular orbital (HOMO)-lowest unoccupied molecular orbital (LUMO) gap can act like a semiconductor with short band gap.<sup>85</sup> Even though this review focuses on plasmonic NPs, it is important to highlight that metal clusters can also be used as co-absorbers to enhance the absorption of metal oxides.<sup>86</sup>

**4.1.2.3. NP shape.** Varying particle shape enables tuning of the NP LSPR frequency, which makes possible to absorb and utilize light throughout the complete solar spectrum. In addition, it has been suggested that NP shape also affects the amount and location of generated hot carriers within the NP.<sup>87,88</sup> Harutyunyan *et al.*<sup>87</sup> studied the hot charge carrier dynamics with standard pump-probe measurements for different nanostructure geometries and reported ultrafast dynamics in nanostructures with “hot spots” (areas with greatly enhanced electromagnetic field). The authors ascribed this ultrafast response to an efficient generation of hot electrons from hot spots. In good agreement with this, Sousa-Castillo *et al.*<sup>88</sup> showed that the photochemical response of TiO<sub>2</sub> is enhanced to a larger extent when functionalized with nanostars than when functionalized with nanorods or spherical NPs. The high photocatalytic activity was ascribed to hot spots present around the spikes of the NP, which promotes the hot carrier generation near the NP-semiconductor interface and the subsequent HEI to the semiconductor.

As will be explained in the following section, the HEI mechanism is the only known plasmonic mechanism that can expand the absorption of a semiconductor water splitting device to longer wavelengths without depending on spectral overlap with the semiconductor. Therefore, if well-defined plasmonic NPs that absorb light beyond the semiconductor absorption edge are used, the HEI can be studied independently, as was done in the works discussed above. However, in most reports on plasmonic water splitting, an overlap between the semiconductor absorption and the NP absorption/scattering may give rise to many other plasmonic and non-plasmonic effects that simultaneously affect the semiconductor absorption and electrochemical properties.<sup>27,28,55,56,89–97</sup> These ideas are discussed in the context of recent literature reviewed in the following two sections.

## 4.2. Light scattering, light concentration and PIRET

Unlike the HEI mechanism, the light scattering, light concentration and PIRET mechanisms do not transfer the plasmon



energy by charge transfer, but radiatively or by a dipole-dipole interaction, inducing interband excitations in a neighbouring semiconductor. The benefits of these mechanisms in photoelectrochemical water splitting are illustrated in Fig. 15 for backside illumination (light reaching the semiconductor first). Most bare semiconductor films exhibit incomplete absorption and the transmitted light is unexploited (Fig. 15A). When the semiconductor is decorated with light scattering NPs (cf. Fig. 15B), the transmitted light interacts with the metal NPs, inducing surface plasmons that subsequently decay by scattering the photons back into the semiconductor. As a result, the optical path length through the semiconductor is increased, which increases its absorption and water splitting performance.<sup>22</sup> Fig. 15C illustrates a similar principle, where the transmitted light induces LSPR in the metal NP, which generates a highly localized electric field in the vicinity of the NP. This NP near-field can locally excite additional electrons from the valence band of the semiconductor to the conduction band (*i.e.*, through the light concentration and PIRET mechanisms), again, improving the device performance.

Essentially, light concentration and light scattering only increase the interaction of light with the semiconductor by

concentrating it and by increasing its path through the semiconductor. Therefore, these mechanisms are called light trapping or photonic enhancement mechanisms. They can increase the absorption of the semiconductor for plasmonic NP systems with resonances with energies above the optical band gap edge (OBGE) of the semiconductor.<sup>46,51</sup> PIRET, as with light concentration and light scattering, also occur at wavelengths that overlap with the semiconductor's absorption spectra. However, PIRET has also been demonstrated to generate electron-hole pairs below the semiconductor OBGE, suggesting strong dipole-dipole coupling with band edge states that are optically inaccessible (see Section 4.2.2).<sup>25,74</sup>

**4.2.1. Light scattering.** An important characteristic of light scattering plasmonic NPs is that the light is scattered preferentially towards the surrounding material that has the largest refractive index.<sup>98</sup> Therefore, when a metal NP is placed on the semiconductor/electrolyte interface (Fig. 15B), light is scattered preferentially towards the semiconductor, since they generally have a larger refractive index (RI, *e.g.*, RI  $\sim 2.5$  for BiVO<sub>4</sub>, RI  $\sim 2.6$  for TiO<sub>2</sub> and RI  $\sim 2.9$  for Fe<sub>2</sub>O<sub>3</sub>) than an aqueous electrolyte (RI  $\sim 1.3$ ). We recently<sup>22</sup> demonstrated a purely scattering effect by decorating the surface of BiVO<sub>4</sub> photoanodes with light

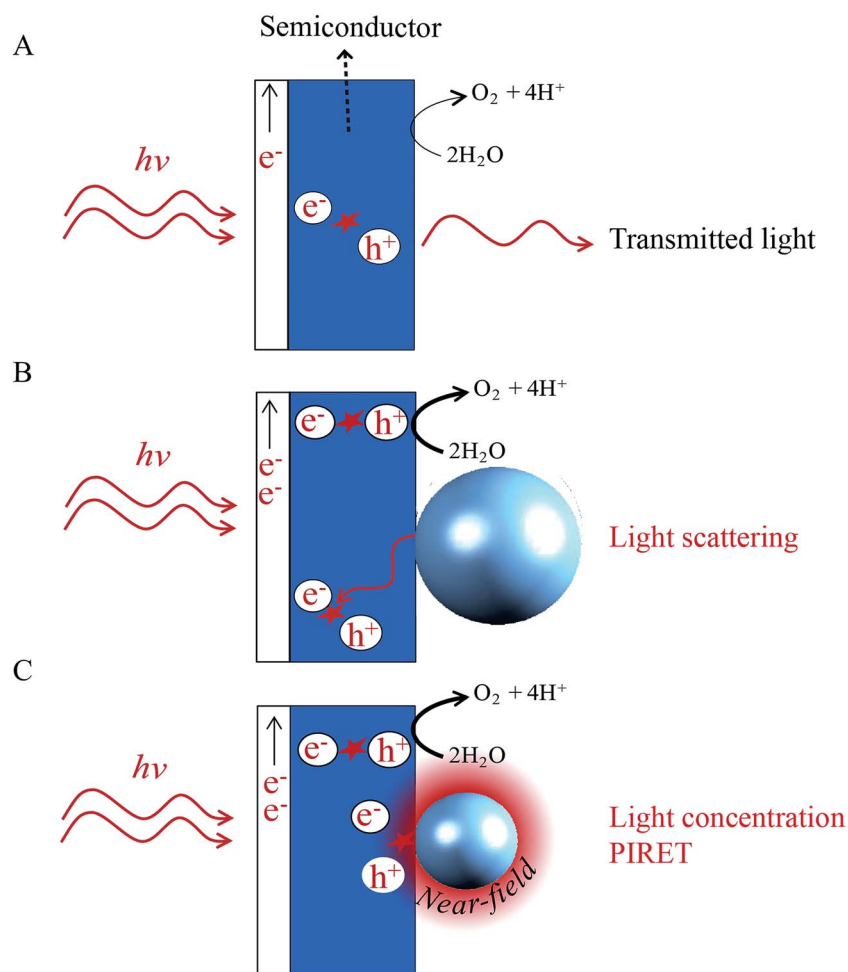


Fig. 15 Illustration of absorption enhancement in a water splitting photoanode due to light scattering, light concentration and PIRET.



scattering 65 nm silver NPs. Fig. 16A shows the increase in absorption of  $\sim 100$  nm  $\text{BiVO}_4$  grains after NP deposition. It can be clearly seen that the absorption increases only within the semiconductor light absorption range and according to the absorption coefficients of the semiconductor. This suggests that the NPs only absorb negligible light on their own and preferentially scatter the light back to be absorbed by the semiconductor. If the decorating NPs would, instead, be absorbing light and subsequently releasing the energy to the surroundings (e.g., releasing heat), the measured absorption increase would be expected to be only proportional to the surface plasmon resonance curve and not to the semiconductor absorption spectrum. In order to investigate the effect of this absorption increase on the conversion efficiency of the device, IPCE measurements were carried out with and without adding a hole scavenger in the electrolyte (cf. Fig. 16B). The IPCE increase upon NP functionalization without the hole scavenger may be due to the contribution of two beneficial effects: (i) surface effects (e.g., increase catalysis) and (ii) bulk effects (e.g., absorption increase due to the light scattering mechanism). On the other hand, with the addition of the hole scavenger, the hole transport from the semiconductor surface to the electrolyte (i.e., surface effects) is no longer rate limiting and, therefore, any change in the IPCE after NP deposition can be assigned to

a bulk effect (e.g., increase in absorption).<sup>99</sup> We therefore assigned the IPCE increase with  $\text{H}_2\text{O}_2$  (hole scavenger) shown in Fig. 16B to the absorption increase shown in Fig. 16A. In the same work, an even larger absorption increase ( $\sim 6\%$ ) was obtained for front illumination (light reaching the NPs first), demonstrating that the preferential scattering mechanism can reduce the reflected light at the semiconductor–electrolyte interface.

#### 4.2.2. Near-field effects: light concentration and PIRET.

Plasmonic NPs with large absorption cross sections (cf. Section 2.1) can act as efficient light concentrators.<sup>51,100–102</sup> In the light concentration mechanism the NP near-field energy is radiatively transferred to the semiconductor, locally generating electron–hole pairs in the semiconductor.<sup>20</sup> As with direct light excitation, in this near-field effect the electron–hole formation rate in the semiconductor is proportional to the local intensity of the electric field (i.e.,  $|E|^2$ ). This is an important feature of this mechanism, since it allows the ability to locally increase the electron–hole generation by orders of magnitude due to the extreme field enhancements that can be achieved around plasmonic NPs (cf. Section 2.3).<sup>53</sup> Moreover, concentrating the light allows the ability to promote electron hole pair generation in specific/predefined regions of the semiconductor film, where the photogenerated charge carriers are expected to be efficiently separated (e.g., space charge region, see discussion below). Since this plasmon-induced absorption occurs due to the near-field interaction with the semiconductor, the probability of absorption is expected to increase with the plasmon life-time.<sup>103</sup> Moreover, it was suggested that for this mechanism to be effective, the reciprocal of the surface plasmons life-time (decay rate) must be smaller than the rate of absorption of the semiconductor.<sup>51</sup> Therefore, this antenna effect is limited by the decay of the surface plasmons through other competing damping processes (e.g., intraband and interband excitations in the metal).<sup>21</sup>

Cushing *et al.*<sup>25</sup> discovered that, unlike direct light excitation, the plasmon's strong dipole moment can also locally induce excitations below the OBGE, extending the light utilization of the semiconductor to longer wavelengths. In this near-field mechanism, called PIRET, the surface plasmon decays through a non-radiative dipole–dipole energy transfer to the semiconductor, resulting in electron–hole excitations in the semiconductor. This mechanism was studied in an Au– $\text{SiO}_2$ – $\text{Cu}_2\text{O}$  sandwich NP (Fig. 17A) by transient absorption spectroscopy (TAS) and wavelength dependent photocatalysis. In this study the insulating  $\text{SiO}_2$  layer prevent HEI from the metal to the semiconductor outer layer (i.e.,  $\text{Cu}_2\text{O}$ ), while the near-field can still penetrate the  $\text{SiO}_2$  layer and interact with the semiconductor. Wavelength dependent photocatalytic measurements showed a clear enhancement in the conversion efficiency at energies both above and below the semiconductor OBGE (Fig. 17B) when compared with the efficiency of the bare semiconductor (Fig. 17C). These results, accompanied by transient analysis and theoretical calculations, lead the authors to identify the PIRET mechanism as being responsible for the observed enhancement. Two important advantageous characteristics of PIRET are that (i) unlike light trapping mechanisms,

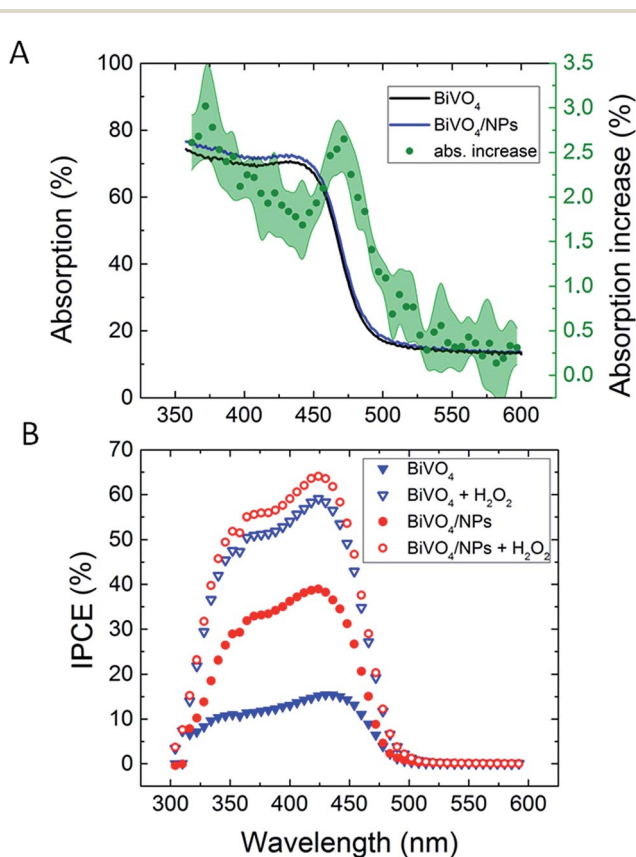


Fig. 16 (A) Back illumination absorption increase in the  $\text{BiVO}_4$  spectra upon deposition of 65 nm Ag NPs. (B) Back illumination Incident photon to current conversion efficiency (IPCE) measurements before and after 65 nm Ag NP functionalization. Reprinted with permission from ref. 22. Copyright 2016 Wiley-VCH.



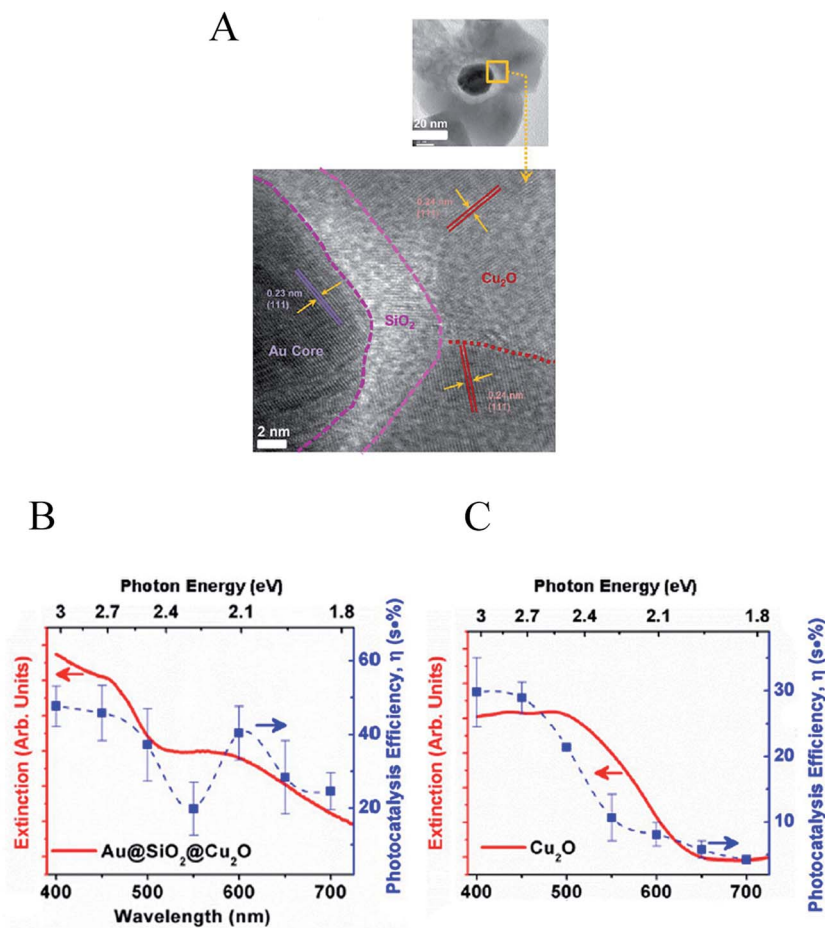


Fig. 17 (A) Au@SiO<sub>2</sub>@Cu<sub>2</sub>O sandwich structure (top) and an enlargement of the micrograph for the interface regions of the sandwich structure shows the various crystal orientations (bottom). Ultraviolet-visible spectra and photocatalytic action spectra for (B) Au@SiO<sub>2</sub>@Cu<sub>2</sub>O and (C) Cu<sub>2</sub>O. Reprinted with permission from ref. 25. Copyright 2012 ACS.

it allows for absorption enhancement of the semiconductor at energies below its OBGE due to dipole-dipole coupling to weak band edge states (yet still requiring a spectral overlap with the semiconductor absorption) and (ii) unlike HEI, it does not require specific band energy alignment of the semiconductor with respect to the Fermi level of the plasmonic NP. The discovery of PIRET modifies the previous understanding of the light concentration mechanism since the localization of the incident electromagnetic field in the vicinity of the NP (NP near-field) cannot only induce electron-hole pairs radiatively (proportionally to the square of the electric field) but can also non-radiatively induce electron-hole pairs below the OBGE in the near-field through a dipole-dipole interaction (PIRET). Since PIRET is a relatively new discovery, most water splitting publications that use small light absorbing NPs to locally increase the semiconductor absorption discuss their results solely under the context of the light concentration mechanism, and should be revisited including PIRET in the interpretation.

For small light absorbing NPs, it is still not clear what percentage of the surface plasmons energy is transferred to the semiconductor through near-field mediated energy transfer (e.g., PIRET) and what percentage is through HEI. However,

recently, Cushing *et al.*<sup>54</sup> shed light on this issue by studying the charge carrier dynamics in TiO<sub>2</sub> coated silver NPs with transient absorption spectroscopy (TAS). The authors report that in these coated NPs, HEI and PIRET take place simultaneously, with PIRET being the more prominent mechanism. This points out the fact that the HEI is generally more limited than PIRET, due to its strict dependence on several operating parameters (*cf.* Section 4.1, e.g., Schottky energy barrier). In the same work, Cushing *et al.*, also studied other coated NP architectures with transient absorption analysis, finding the conditions needed for HEI and PIRET to occur in a plasmonic NP/semiconductor composite as summarized in Fig. 18. Their findings confirm that (i) unlike HEI, PIRET only takes place at the region of the spectrum where there is spectral overlap between the semiconductor and the NP and (ii) unlike HEI, PIRET can occur even when there is not direct contact between the NP and the semiconductor, since the NP near-field can penetrate through a thin insulating layer. Due to the latter, plasmonic NPs with an insulating coating block the HEI mechanism and, therefore, facilitates the study of PIRET and the light concentration mechanisms. Combined with additional reasons described below, this has led to a significant number of publications that



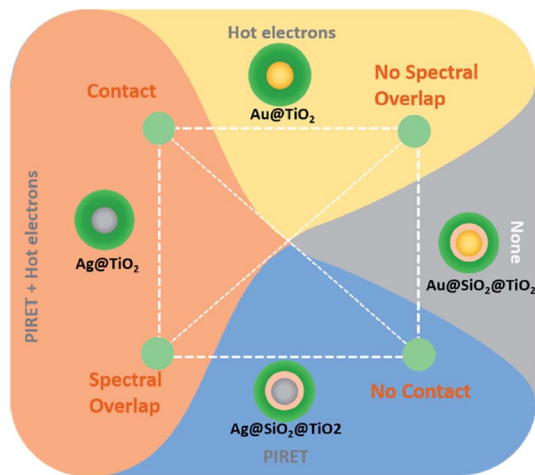


Fig. 18 Variables that control the possible plasmonic enhancement near-field mechanisms for extending photoconversion. Connecting the line between the properties of the given core@shell nanoparticle gives the corresponding enhancement mechanisms present. Reprinted with permission from ref. 54. Copyright 2015 ACS.

use plasmonic NPs coated with an insulating layer in NP/semiconductor composite water splitting devices.<sup>55,89,104</sup>

Thomann *et al.*,<sup>104</sup> functionalized  $\text{Fe}_2\text{O}_3$  films with 50 nm gold NPs coated with a 10 nm shell of  $\text{SiO}_2$  in two configurations that have the (i) NPs embedded in the film and (ii) the NPs at the semiconductor–electrolyte interface. Both configurations showed a clear enhancement in the wavelength dependent photocurrent compared with the bare semiconductor sample. The spectra of this photocurrent enhancement closely followed the simulated absorption increase due to the plasmonic NPs, which evidenced a plasmonic effect for both configurations. This photocurrent enhancement was assigned, with the help of full-field electromagnetic simulations, to the semiconductor absorption increase in the vicinity of the plasmonic NPs. However, for configuration (ii) (NPs at the semiconductor surface) a background wavelength independent enhancement was seen, which could not be explained by plasmonic mechanisms such as PIRET or light trapping. The authors speculate that such wavelength independent enhancement arise from surface effects such as catalytic effects on water oxidation by the NPs.

Abdi *et al.*,<sup>55</sup> decorated the surface of  $\text{BiVO}_4$  photoanode films with 50 nm  $\text{SiO}_2$  coated Ag NPs and found a 2.5-fold photocurrent enhancement under simulated sun illumination at 1.23 V vs. RHE. The authors ascribed this enhancement to both catalytic and optical effects due to the decorating plasmonic NPs. By adding a hole scavenger ( $\text{H}_2\text{O}_2$ ) in the electrolyte, the authors were able to identify the absorption enhancement contribution to the total IPCE enhancement. An absorption enhancement of 33% was in good agreement with full-field electromagnetic simulations and was ascribed to far-field (light scattering) and, in a lesser extent, to near-field effects. As can be seen in Fig. 19, the IPCE increase reported in this work is larger than 15% IPCE at  $\sim 425$  nm. Such a large IPCE enhancement can be explained by the significant overlap between the

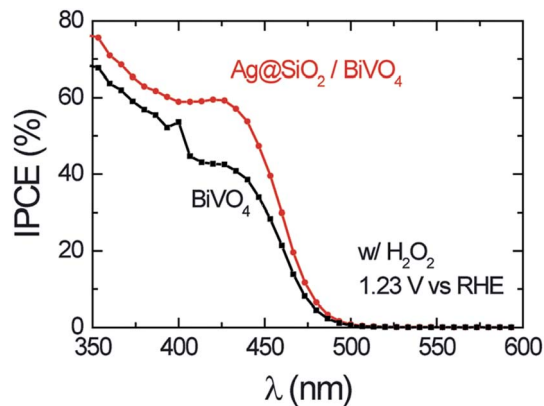


Fig. 19 IPCE of bare  $\text{BiVO}_4$  and  $\text{Ag@SiO}_2/\text{BiVO}_4$  at 1.23 V vs. RHE in the presence of 0.5 M  $\text{H}_2\text{O}_2$  in the electrolyte. Reprinted with permission from ref. 55. Copyright 2014 RSC.

semiconductor and the plasmonic NPs absorption spectra, which is a requirement for the light trapping mechanisms (concentration and scattering of light) and PIRET. In order to increase such spectral overlap, the NPs' geometry,<sup>89</sup> composition<sup>89</sup> and their spatial distribution (*e.g.*, dimer formation<sup>22,30</sup>) can be modified. As example, Erwin *et al.*<sup>89</sup> synthesized Au–Ag core–shell nanostructures to expand the absorption overlap of the NP with the semiconductor. When compared with the absorption of spherical NPs, the Au–Ag core–shell nanostructures (*e.g.*, nanopillars) exhibited a second absorption mode and broader absorption spectra. These particles were coated with a thin insulating layer of  $\text{SiO}_2$  and embedded in mesoporous  $\text{TiO}_2$  photoanodes. The absorption and IPCE of the bare  $\text{TiO}_2$ , Au–Ag core–shell nanostructures/ $\text{TiO}_2$  composite and spherical Au NPs/ $\text{TiO}_2$  composite are shown in Fig. 20. The Au–Ag core–shell nanostructures clearly increased the absorption of the photoanode in a larger extent than the spherical Au NPs, throughout the measured range. Accordingly, the IPCE enhancement was also increased in a larger extent for the Au–Ag core–shell nanostructures/ $\text{TiO}_2$  composite. This shows that broadening the absorption overlap between the NP and the semiconductor by modifying the NP geometry and composition can efficiently extend the action of light trapping and PIRET. However, the obtained IPCE increase was low ( $\sim 0.01\%$ , Fig. 20B) due to the poor visible light absorption of  $\text{TiO}_2$  (Fig. 20A). In the same work, the authors also characterized their samples by measuring the photocurrent under solar simulated light, modulated at different light intensities (*i.e.*, from  $50 \text{ mW cm}^{-2}$  to  $300 \text{ mW cm}^{-2}$ ). While the bare photocurrent of the semiconductor showed a half order dependency to the light intensity, the photocurrent of the functionalized composites showed a first order dependency. This phenomenon was previously reported<sup>46</sup> for  $\text{TiO}_2$  samples functionalized with Ag NPs, and can be explained by the near-field mechanisms.<sup>20</sup> These mechanisms concentrate the light at the semiconductor/electrolyte interface, increasing the generation of charges near the semiconductor surface where the space charge region is located. Therefore, all the near-field induced charges are efficiently separated due to the built-in electric field in the space



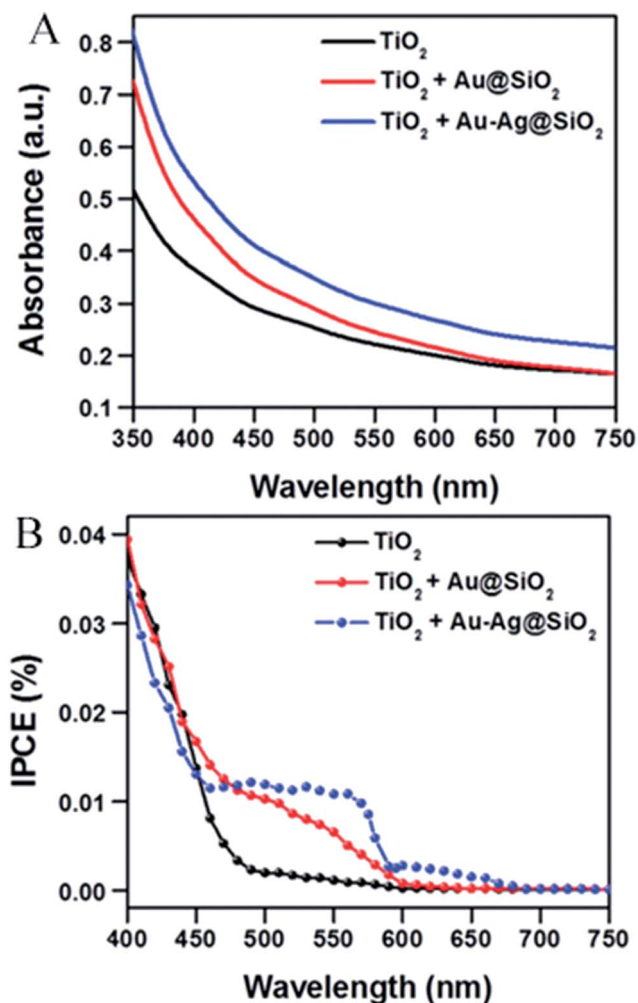


Fig. 20 (A) Absorption spectra showing enhancement in light absorption with Au-Ag@SiO<sub>2</sub> nanostructures (blue) and Au@SiO<sub>2</sub> nanoparticles (red) embedded within the mesoporous TiO<sub>2</sub> photoanodes relative to TiO<sub>2</sub> only anodes (control, black). (B) IPCE curves of nonenhanced (TiO<sub>2</sub> only) and plasmon enhanced photoanodes. The plasmon enhanced photoanodes are at the optimized concentration. Reprinted with permission from ref. 89. Copyright 2014 RSC.

charge layer. Consequently, in composites where the near-field induced charges are prominent contributors to the total photocurrent, the bulk charge separation is not a limiting step

and the photocurrent shows a first order dependence on light intensity. This important feature of promoting the generation of charges at the space charge region was also studied by Valenti *et al.*,<sup>28</sup> by comparing the light absorption increase of CuWO<sub>4</sub> films when plasmonic NPs were deposited either (i) at the back contact/semiconductor interface or (ii) at the semiconductor/electrolyte interface. It was found that the increase in absorption was more effectively extracted as photocurrent when the NPs were placed at the surface of the semiconductor (ii). This result can again be explained by the efficient separation of the near-field induced charges at the space charge region. Naldoni *et al.*<sup>105</sup> also studied the effect of plasmonic NPs at the semiconductor–electrolyte interface and their findings suggest that both decreasing the interparticle distance and partially embedding the NPs in the semiconductor can enhance the light concentration in the semiconductor and its photocatalytic activity.

It is important to highlight that the near-field induced charge carriers are not only well separated (due to the electric field of the space charge region) but also the hole (in the case of n-type semiconductors) can readily reach the semiconductor/electrolyte interface in the vicinity of the NP, where other plasmonic or non-plasmonic effects can enhance its injection efficiency to the electrolyte (*cf.* Section 5.1). Therefore, the light concentration and PIRET effects are promising tools that could effectively enhance the absorption, bulk separation and injection efficiency to the electrolyte.

In addition to discrete NPs, nanotextured and flat metallic films have also been used to increase the semiconductor light absorption at specific regions of a neighbouring semiconductor.<sup>90,106,107</sup> The increase in absorption for such systems is (i) related to the evanescent fields of the surface plasmon polaritons (SPPs) of nanotextured films,<sup>90,108</sup> or (ii) due to the ability of metal films to reflect light and generate resonant cavity modes.<sup>107</sup> In both cases, the films can also be used as back contact current collector in the water splitting device.<sup>90,107</sup> A synergetic approach combines the LSPR effects provided by plasmonic NPs at the electrolyte–semiconductor interface with additional enhancement mechanisms provided by a metallic film used as back contact. Fang *et al.*<sup>106</sup> showed that this configuration enables light to be efficiently trapped by scattering-reflecting back and forth through the semiconductor between Au nanodisk and a Au mirror film.

Table 1 Optical, physical and electronic characteristics of the plasmonic mechanisms that increase the overall absorption of semiconductor photoelectrodes

	Light scattering	Light concentration	PIRET	HEI
Origin of enhancement		Photonic enhancement		
NP-semiconductor spectral overlap		Required	Dipole–dipole energy transfer	Charge transfer
Enhancement above optical bandgap edge		✓	Required	Not required
Enhancement below optical bandgap edge		✗	✓	✓
NP-semiconductor contact		Not required	Not required	Required
Alignment of band energies		Not required	Not required	Required



Table 1 summarizes the most important physical, optical and electronic characteristics of the above described LSPR mechanisms (*i.e.*, light scattering, light concentration, HEI and PIRET) that can increase the overall absorption of a semiconductor photoelectrode. This table can be used in the design of a plasmonic NP/semiconductor composite photoelectrode to optimize the performance of the semiconductor or to further elucidate the nature of these plasmonic mechanisms.

## 5. Electrochemical effects

Besides light absorption, plasmonic NP can also induce effects in the semiconductor's charge transfer properties (*cf.* Subsection 5.1.), energetics (*cf.* Subsection 5.2.), and band structure (*cf.* Subsection 5.3.). In this section we discuss these plasmon-induced and non-plasmon-induced NP effects that do not increase light absorption, but instead facilitate the electrochemical processes in a semiconductor-based water splitting device.

### 5.1. Effects on charge transfer

Depending on where the plasmonic NPs are placed in the semiconductor device (embedded or on the surface), the NPs can affect the bulk and/or surface charge transfer processes that the photogenerated charge carriers undergo in the semiconductor to carry out the water splitting half reactions.<sup>27,28</sup> In the case of n-type semiconductor photoanodes, the photogenerated holes first move through the semiconductor towards the semiconductor surface (bulk charge transport). Subsequently, the hole needs to be transferred from the valence band to the semiconductor surface, where the hole is injected to the electrolyte to evolve oxygen. In particular this last step (charge injection from the semiconductor surface to the electrolyte) has often been ascribed as main responsible for photocurrent increase upon plasmonic NP functionalization.<sup>22,27–29,109–113</sup> Haro *et al.*,<sup>27</sup> obtained a significant increase in the catalysis and, in a lesser extent, an increase in the bulk conductivity after embedding gold NPs in a mesoporous TiO<sub>2</sub> photoanode. After discarding HEI and light trapping mechanisms (based on PEC characterization), the authors studied the influence of the NPs on the bulk conductivity, chemical capacitance and surface charge transfer resistance of the TiO<sub>2</sub> with electrochemical impedance spectroscopy (EIS) analysis. In this technique, the impedance (complex voltage to current ratio) spectrum of the system is obtained by applying a bias AC voltage to the PEC cell at different frequencies and recording the current response. Subsequently, the impedance spectrum is modelled with an equivalent circuit (EC), consisting of capacitors and resistors, that represents the limiting transport processes in a well-known PEC system. Haro *et al.*,<sup>27</sup> used a well-established transmission line model as EC to fit the impedance spectra at different applied potentials. The parameters for the surface charge transfer, chemical capacitance and bulk conductivity were extracted from the fittings, as shown in Fig. 21. It can be clearly seen that the charge transfer resistance at the surface progressively decreased with the NP load in the photoanode. The

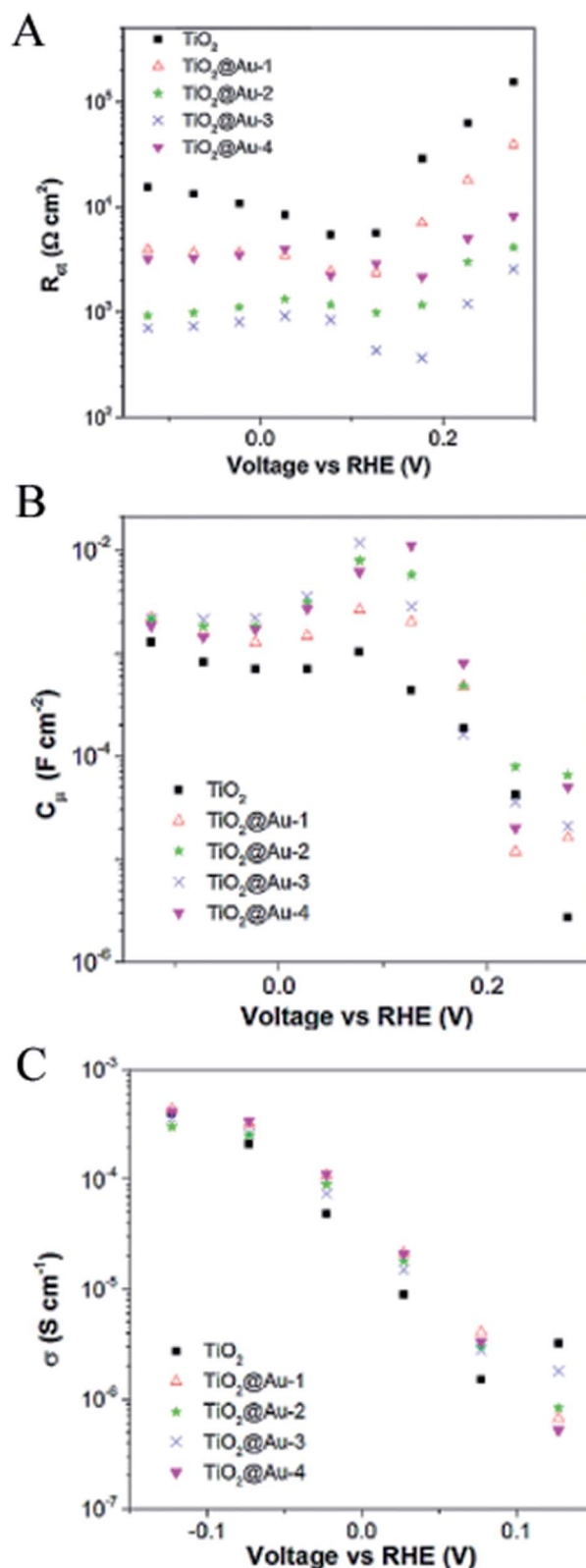


Fig. 21 (A) Charge transfer resistance, (B) chemical capacitance, and (C) conductivity of mesoporous TiO<sub>2</sub> films without and with different loading of Au NPs under illumination at  $100 \text{ mW cm}^{-2}$ . The conductivity has been only calculated in the potential range where the transmission line is observed. Reprinted with permission from ref. 27. Copyright 2014 Elsevier Ltd.



chemical capacitance also increased upon NP functionalization, which is explained in this work by the increase of the density of states due to the gold NPs. Finally, Fig. 21C shows that the bulk conductivity slightly increased with the NP load.

The increase in the charge carrier injection to the electrolyte could be due to the inherent catalytic properties of the metal, Fermi level equilibration<sup>59</sup> (cf. Section 5.2.1.) or due to plasmonic effects, such as plasmonic heating,<sup>57</sup> improved adsorption of polar molecules that align in the direction of the NP near-field<sup>58</sup> and hot electron induced activation of co-catalysts.<sup>114</sup> While EIS is a powerful tool that allows the ability to quantify the resistance of the charge injection to the electrolyte, other techniques must be developed in order to elucidate and distinctly recognize the different plasmonic and non-plasmonic effects that facilitate the charge transport processes. These charge transfer effects are of extreme importance when they occur in combination with plasmonic mechanisms that increase the absorption of the semiconductor, since for this case the NP plays the dual role of (i) light absorber and (ii) co-catalyst. This dual effect has already been demonstrated in different NP/semiconductor systems where the NP facilitate the charge carrier transport and also enhance the absorption through HEI<sup>18</sup> or light trapping.<sup>22,40</sup> In particular for near-field effects (light concentration and PIRET) occurring near the semiconductor surface, the additional plasmonic induced charge carriers (i) are well separated due to the space charge region, (ii) more readily reach the semiconductor surface, and (iii) exhibit enhanced charge injection to the electrolyte due to the enhanced catalysis near the NP. In this way, near-field induced charge carriers are expected to efficiently contribute to the overall photocurrent.

## 5.2. Effects on energetics

**5.2.1. Semiconductor-metal Fermi level equilibration.** In a photoelectrochemical cell, the semiconductor photoelectrode Fermi level equilibrates with the redox couple in the electrolyte (n-type semiconductors equilibrate with oxidation potentials and p-type semiconductors equilibrate with reduction potentials). When a n-type semiconductor is illuminated with light, electron-hole pairs are generated and the Fermi level shifts to more negative potentials. The difference between the Fermi level in the dark and under illumination determines the internal photovoltage.<sup>115</sup> Similarly, when a metallic NP/semiconductor composite photoelectrode is used, the Fermi level equilibrates between the metal, semiconductor and redox couple. Interestingly, when the metallic NP/semiconductor composite is illuminated, the Fermi level of the composite can have an even larger negative shift (compared to the bare semiconductor) due to the ability of metallic NPs to store the photogenerated electrons coming from the semiconductor (cf. Fig. 22).<sup>59</sup> The transfer of electrons from the excited semiconductor to the NP continues until photoequilibrium between the metal and the semiconductor is obtained. Such a metallic NP induced negative shift in the Fermi level results in an increased photovoltage and photocatalytic activity (cf. Fig. 22).<sup>59,116</sup>

A clear correlation between the extent of the negative induced Fermi level shift and the increased catalytic activity was

shown by Subramanian *et al.*<sup>59</sup> The authors decorated TiO<sub>2</sub> NPs with Au NPs of different diameters (*i.e.*, 3-, 5- and 8 nm) and found that decreasing NP size consistently increased the Fermi level negative shift and the photocatalytic activity of the composite. The increase of the Fermi level shift with decreasing NP size could be explained by the discrete nature of the energy levels in Au NPs, which results in a larger shift in energy level per stored electron for the smaller NPs.<sup>59</sup>

This subsection shows that metallic plasmonic NPs can not only increase the absorption of the semiconductor and improve its charge transfer properties, but they can also alter its electronic band energetics. Since properties like the plasmonic NP size determine the efficiency of both (i) plasmonic mechanisms that increase the semiconductor absorption, and (ii) non-plasmonic mechanisms that improve the energetics, a trade-off typically needs to be made according to the specific semiconductor limitations.

**5.2.2. HEI induced Fermi level shift.** The work of Chen *et al.*<sup>26</sup> and Mubeen *et al.*<sup>23</sup> (see Section 4.1.) demonstrate that the oxygen and hydrogen evolution reactions on NP/semiconductor composite photoelectrodes can be driven by hot holes and hot electrons, respectively. However, Shi *et al.*<sup>56</sup> recently suggested that hot electrons and holes can improve the performance of water splitting electrodes in other ways apart from directly driving the water splitting half reactions. They report an increase in the electrocatalytic activity (*i.e.* higher current at lower over-potentials) for the hydrogen evolution reaction on MoS<sub>2</sub> upon gold nanorod decoration. This increase is explained by a change in the MoS<sub>2</sub> Fermi level due to hot electron injection from the illuminated gold nanorods to the semiconductor (*i.e.*, MoS<sub>2</sub>). The absorption spectra of the materials synthesized in this work are shown in Fig. 23A. The nanorod-decorated material (Au-MoS<sub>2</sub>) exhibit a LSPR longitudinal absorption mode of the gold nanorods at 813 nm. The electrocatalytic activity of the synthesized materials without illumination, using a typical three-electrode configuration, is shown in Fig. 23B together with the activity of the Au-MoS<sub>2</sub> composite under illumination with an 808 nm laser. The result of interest for this review is the positively shifted onset potential (from -0.22 to -0.16 V *vs.* RHE) when the composite electrode

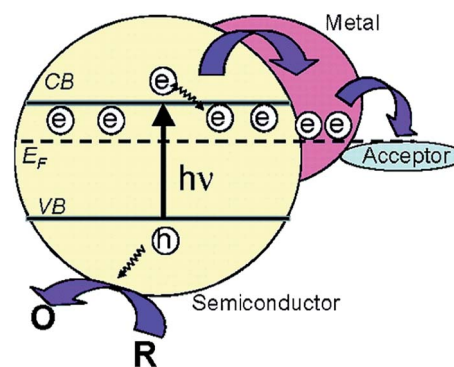


Fig. 22 Fermi level equilibration in a semiconductor-metal nano-composite system. Reprinted with permission from ref. 59. Copyright 2004 ACS.



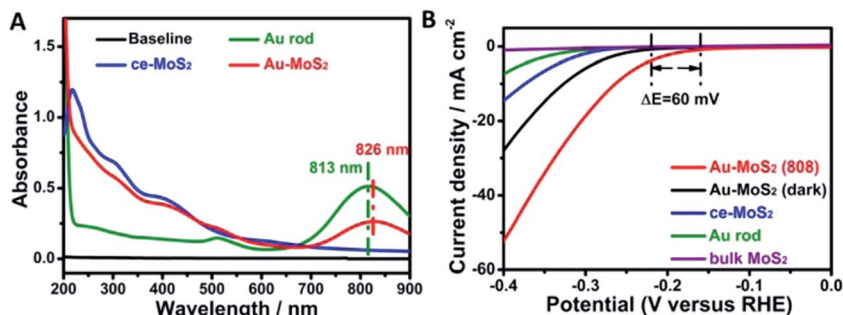


Fig. 23 (A) UV-vis spectra of MoS<sub>2</sub> (ce-MoS<sub>2</sub>) nanosheet, gold nanorod and Au–MoS<sub>2</sub>. (B) Hydrogen evolution reaction polarization curves obtained on several catalysts as indicated. Reprinted with permission from ref. 56. Copyright 2015 ACS.

(i.e., Au–MoS<sub>2</sub>) is illuminated with the 808 nm laser. The activity of this composite was also tested with 532 nm and 650 nm lasers but no activity improvement was observed. The fact that activity only improved under illumination with the light energy that corresponds to the LSPR mode (i.e., 808 nm, cf. Fig. 23A), strongly suggests a surface plasmon resonance effect. Moreover, *in situ* electrochemical LSPR scattering measurement under a dark-field microscope suggest hot electron injection from the Au nanorod to the MoS<sub>2</sub> semiconductor. Based on these results, Shi *et al.* propose the mechanism illustrated in Fig. 24A (following the processes I, III and V) to explain the observed enhancement (Fig. 23B). Process I represents the hot electron–hole formation due to the non-radiative SPR decay. The hot electron could then recombine within the NP (process II), be injected to the conduction band of the semiconductor (process III) and be injected to the electrolyte to drive the hydrogen evolution reaction (process IV). The authors discard this last option (IV) as a main process, since gold is not a good hydrogen evolution catalyst. The hot electron injection to the semiconductor's conduction band (process III) is a more likely process to occur due to the low Schottky barrier between gold and MoS<sub>2</sub>. Once in the semiconductor conduction band, the hot electron could then be injected back into the electron-deficient NP (process V in Fig. 24A). The continuous hot electron injection to the conduction band of the semiconductor increases its Fermi level (cf. Fig. 24B), bringing it closer to the energy level of the redox pair H<sup>+</sup>/H<sub>2</sub>. This effect can decrease the overpotential of the semiconductor for the hydrogen evolution reaction as observed by the authors

(cf. Fig. 23B). Finally, different hole scavengers were added to the electrolyte in order to avoid charge recombination in the gold nanorod (process II in Fig. 24A), which would in turn promote the hot electron injection to the semiconductor. In accordance with the suggested mechanism, the use of hole scavengers (e.g., ethanol, methanol, glucose) provided higher current densities. More specifically, ethanol further lowered the onset potential of the composite under laser illumination as much as –0.12 mV. These results show that plasmonic NP decoration can also increase the catalytic activity of semiconductors and promises to be a key component towards the replacement of precious metals (e.g., platinum) as catalyst electrodes for the hydrogen evolution reaction in water splitting devices.

### 5.3. Effects on band structure

Finally, Chen *et al.*,<sup>26</sup> studied the influence of gold NPs' near-field on the conduction/valence band of ZnO nanorods (same system discussed above in Section 4.1.) with X-ray absorption near edge structure (XANES). In this study, the gold NPs (with sizes of 4.7 nm ± 0.7 nm) were sitting uniformly on the surface of the ZnO nanorods. With XANES the authors observed a significant increase in the ZnO conduction band vacancies under plasmon-induced illumination, which can promote the separation of photogenerated electrons and holes. Such changes in the band structure near the NP/semiconductor interface were ascribed to the NP near-field. Therefore, the authors show that two advantageous plasmonic effects can

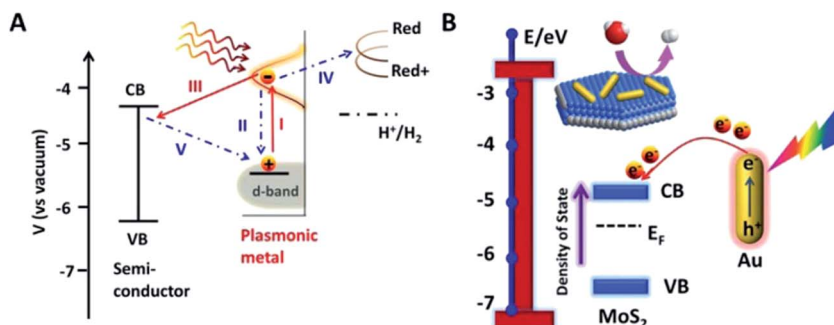


Fig. 24 (A) Different plausible hot electrons transfer pathways likely to occur during SPR. (B) Schematic Au–MoS<sub>2</sub> and energy level diagram illustrating hot electrons injection and change of MoS<sub>2</sub> Fermi level. Reprinted with permission from ref. 56. Copyright 2015 ACS.



occur in a plasmonic NP/semiconductor composite: (i) near-field induced generation of vacancies in the conduction band, and (ii) absorption increase through HEI (*cf.* Section 4.1.).

## 6. Conclusions and outlook

Significant progress has been made in the last several years to elucidate the mechanisms (*i.e.*, light scattering, light concentration, PIRET and HEI) by which plasmonic NPs can improve the solar light utilization of semiconductor photoelectrodes for efficient solar water splitting. Research on metal oxide water splitting photoelectrodes, which exhibit good catalytic activity and stability in aqueous media, benefits particularly from these new plasmonic mechanistic insights to circumvent the specific optical weaknesses of the different metal oxides. Table 1 summarizes some of the most important characteristics of each plasmonic mechanism that can enhance the light utilization in NP/semiconductor water splitting devices. As shown in this table, PIRET and HEI are mechanisms that can extend the light utilization of metal oxide photoelectrodes with large bandgap energies to the visible and near-infrared light. In particular, the HEI mechanism, whose efficiency is independent of the semiconductor absorption, allows for light harvesting of the entire solar irradiation spectrum by, for example, using rod NPs with different geometrical aspect ratios that collectively absorb light throughout the solar irradiation spectrum. However, the HEI mechanism suffers from many requirements, including the adequate alignment of the semiconductor band energies with respect to the Fermi level of the metal NP, which restricts its use to a limited number of material combinations. By contrast, photonic enhancements and PIRET do not require any band alignment, but their efficiency strongly depends on the NP-semiconductor spectral overlap. Therefore, following the great advances in the synthesis of well defined NPs and NPs systems (*e.g.*, NP dimers, NP-metallic films systems, *etc.*) with predefined absorption spectra, more research needs to be directed towards ideal spectral overlap to achieve complete light absorption in promising new metal oxides with short band gaps by means of photonic enhancement and PIRET.

While significant progress has been made in the understanding of the mechanisms to increase the light utilization of metal oxides, less attention has been paid to other roles that plasmonic NPs play when used in high performing metal oxide photoelectrodes (*e.g.*, as a catalyst, co-catalyst, recombination centers, *etc.*). In particular, metal oxide photoelectrodes operating at low applied biases are often limited by poor bulk or interfacial charge transfer processes that are highly sensitive to the presence of metal NPs. In order to obtain a real optical contribution of plasmonic NP in efficient plasmonic NP/semiconductor water splitting devices, a better understanding of the NP charge transfer and energetics effects in the semiconductor must be further elucidated.

## Acknowledgements

Financial support from the following institutions is gratefully acknowledged: NWO (VENI project granted to Dr Wilson A.

Smith), the Wenner-Gren Foundations, the Swedish Research Council, the Swedish Foundation for Strategic Research, the Royal Swedish Academy of Sciences, the ÅForsk Foundation and the Swedish Government Strategic Research Area in Materials Science on Functional Materials at Linköping University (Faculty Grant SFO-Mat-LiU No 2009 00971).

## References

- 1 A. Fujishima and K. Honda, *Nature*, 1972, **238**, 37–38.
- 2 P. J. Boddy, *J. Electrochem. Soc.*, 1968, **115**, 199–203.
- 3 K. Sivula and R. van de Krol, *Nature Reviews Materials*, 2016, **1**, 15010.
- 4 K. Maeda and K. Domen, *J. Phys. Chem. Lett.*, 2010, **1**, 2655–2661.
- 5 M. A. Butler, R. D. Nasby and R. K. Quinn, *Solid State Commun.*, 1976, **19**, 1011–1014.
- 6 J. Su, L. Guo, N. Bao and C. A. Grimes, *Nano Lett.*, 2011, **11**, 1928–1933.
- 7 R. K. Quinn, R. D. Nasby and R. J. Baughman, *Mater. Res. Bull.*, 1976, **11**, 1011–1017.
- 8 A. Kay, I. Cesar and M. Grätzel, *J. Am. Chem. Soc.*, 2006, **128**, 15714–15721.
- 9 J. Y. Kim, G. Magesh, D. H. Youn, J.-W. Jang, J. Kubota, K. Domen and J. S. Lee, *Sci. Rep.*, 2013, **3**, 2681.
- 10 J.-N. Nian, C.-C. Hu and H. Teng, *Int. J. Hydrogen Energy*, 2008, **33**, 2897–2903.
- 11 A. Paracchino, V. Laporte, K. Sivula, M. Grätzel and E. Thimsen, *Nat. Mater.*, 2011, **10**, 456–461.
- 12 F. F. Abdi, L. Han, A. H. M. Smets, M. Zeman, B. Dam and R. van de Krol, *Nat. Commun.*, 2013, **4**, 2195.
- 13 T. W. Kim and K.-S. Choi, *Science*, 2014, **343**, 990–994.
- 14 X. Shi, I. Y. Choi, K. Zhang, J. Kwon, D. Y. Kim, J. K. Lee, S. H. Oh, J. K. Kim and J. H. Park, *Nat. Commun.*, 2014, **5**, 4775.
- 15 Y. Pihosh, I. Turkevych, K. Mawatari, J. Uemura, Y. Kazoe, S. Kosar, K. Makita, T. Sugaya, T. Matsui, D. Fujita, M. Tosa, M. Kondo and T. Kitamori, *Sci. Rep.*, 2015, **5**, 11141.
- 16 W. J. Youngblood, S.-H. A. Lee, Y. Kobayashi, E. A. Hernandez-Pagan, P. G. Hoertz, T. A. Moore, A. L. Moore, D. Gust and T. E. Mallouk, *J. Am. Chem. Soc.*, 2009, **131**, 926–927.
- 17 M. de Respinis, K. S. Joya, H. J. M. De Groot, F. D'Souza, W. A. Smith, R. van de Krol and B. Dam, *J. Phys. Chem. C*, 2015, **119**, 7275–7281.
- 18 J. Li, S. K. Cushing, P. Zheng, T. Senty, F. Meng, A. D. Bristow, A. Manivannan and N. Wu, *J. Am. Chem. Soc.*, 2014, **136**, 8438–8449.
- 19 P. Zhang, T. Wang and J. Gong, *Adv. Mater.*, 2015, **27**, 5328–5342.
- 20 S. Linic, P. Christopher and D. B. Ingram, *Nat. Mater.*, 2011, **10**, 911–921.
- 21 S. C. Warren and E. Thimsen, *Energy Environ. Sci.*, 2012, **5**, 5133–5146.
- 22 M. Valenti, E. Kontoleta, I. Digdaya, M. Jonsson, G. Biskos, A. Schmidt-Ott and W. Smith, *ChemNanoMat*, 2016, **2**, 739–747.



- 23 S. Mubeen, J. Lee, N. Singh, S. Kramer, G. D. Stucky and M. Moskovits, *Nat. Nanotechnol.*, 2013, **8**, 247–251.
- 24 C. Clavero, *Nat. Photonics*, 2014, **8**, 95–103.
- 25 S. K. Cushing, J. Li, F. Meng, T. R. Senty, S. Suri, M. Zhi, M. Li, A. D. Bristow and N. Wu, *J. Am. Chem. Soc.*, 2012, **134**, 15033–15041.
- 26 H. M. Chen, C. K. Chen, C.-J. Chen, L.-C. Cheng, P. C. Wu, B. H. Cheng, Y. Z. Ho, M. L. Tseng, Y.-Y. Hsu, T.-S. Chan, J.-F. Lee, R.-S. Liu and D. P. Tsai, *ACS Nano*, 2012, **6**, 7362–7372.
- 27 M. Haro, R. Abargues, I. Herraiz-Cardona, J. Martínez-Pastor and S. Giménez, *Electrochim. Acta*, 2014, **144**, 64–70.
- 28 M. Valenti, D. Dolat, G. Biskos, A. Schmidt-Ott and W. A. Smith, *J. Phys. Chem. C*, 2015, **119**, 2096–2104.
- 29 E. Thimsen, F. Le Formal, M. Grätzel and S. C. Warren, *Nano Lett.*, 2011, **11**, 35–43.
- 30 A. Piot, S. K. Earl, C. Ng, S. Dligatch, A. Roberts, T. J. Davis and D. E. Gomez, *Nanoscale*, 2015, **7**, 8294–8298.
- 31 W. R. Erwin, H. F. Zarick, E. M. Talbert and R. Bardhan, *Energy Environ. Sci.*, 2016, **9**, 1577–1601.
- 32 A. Naldoni, F. Riboni, U. Guler, A. Boltasseva, M. Shalaev Vladimir and V. Kildishev Alexander, in *Nanophotonics*, 2016, vol. 5, p. 112.
- 33 S. K. Cushing and N. Wu, *J. Phys. Chem. Lett.*, 2016, **7**, 666–675.
- 34 G. Mie, *Ann. Phys.*, 1908, **25**, 377–445.
- 35 K. L. Kelly, E. Coronado, L. L. Zhao and G. C. Schatz, *J. Phys. Chem. B*, 2002, **107**, 668–677.
- 36 C. Sönnichsen, T. Franzl, T. Wilk, G. von Plessen, J. Feldmann, O. Wilson and P. Mulvaney, *Phys. Rev. Lett.*, 2002, **88**, 077402.
- 37 M. Quinten, in *Optical Properties of Nanoparticle Systems*, Wiley-VCH Verlag GmbH & Co. KGaA, 2011, pp. 55–74, DOI: 10.1002/9783527633135.ch4.
- 38 C. F. Bohren and D. R. Huffman, in *Absorption and Scattering of Light by Small Particles*, Wiley-VCH Verlag GmbH, 2007, pp. 130–157, DOI: 10.1002/9783527618156.ch5.
- 39 N. K. Pathak, G. K. Pandey, A. Ji and R. P. Sharma, *Plasmonics*, 2015, **10**, 1597–1606.
- 40 X. Huang, I. H. El-Sayed, W. Qian and M. A. El-Sayed, *J. Am. Chem. Soc.*, 2006, **128**, 2115–2120.
- 41 S. Kadkhodazadeh, J. R. de Lasson, M. Beleggia, H. Kneipp, J. B. Wagner and K. Kneipp, *J. Phys. Chem. C*, 2014, **118**, 5478–5485.
- 42 P. Nordlander, C. Oubre, E. Prodan, K. Li and M. I. Stockman, *Nano Lett.*, 2004, **4**, 899–903.
- 43 P. K. Jain, W. Huang and M. A. El-Sayed, *Nano Lett.*, 2007, **7**, 2080–2088.
- 44 M. Quinten, A. Leitner, J. R. Krenn and F. R. Aussenegg, *Opt. Lett.*, 1998, **23**, 1331–1333.
- 45 P. L. Stiles, J. A. Dieringer, N. C. Shah and R. P. V. Duyne, *Annu. Rev. Anal. Chem.*, 2008, **1**, 601–626.
- 46 S. Linic, P. Christopher and D. B. Ingram, *Nat. Mater.*, 2011, **10**, 911–921.
- 47 E. Hao and G. C. Schatz, *J. Chem. Phys.*, 2004, **120**, 357–366.
- 48 B. Willingham, D. W. Brandl and P. Nordlander, *Appl. Phys. B*, 2008, **93**, 209–216.
- 49 M. Belkin, S.-H. Chao, M. P. Jonsson, C. Dekker and A. Aksimentiev, *ACS Nano*, 2015, **9**, 10598–10611.
- 50 F. Nicoli, D. Verschuere, M. Klein, C. Dekker and M. P. Jonsson, *Nano Lett.*, 2014, **14**, 6917–6925.
- 51 H. A. Atwater and A. Polman, *Nat. Mater.*, 2010, **9**, 205–213.
- 52 L. Zhang, L. O. Herrmann and J. J. Baumberg, *Sci. Rep.*, 2015, **5**, 16660.
- 53 D. M. Callahan, J. N. Munday and H. A. Atwater, *Nano Lett.*, 2012, **12**, 214–218.
- 54 S. K. Cushing, J. Li, J. Bright, B. T. Yost, P. Zheng, A. D. Bristow and N. Wu, *J. Phys. Chem. C*, 2015, **119**, 16239–16244.
- 55 F. F. Abdi, A. Dabirian, B. Dam and R. van de Krol, *Phys. Chem. Chem. Phys.*, 2014, **29**, 15272–15277.
- 56 Y. Shi, J. Wang, C. Wang, T.-T. Zhai, W.-J. Bao, J.-J. Xu, X.-H. Xia and H.-Y. Chen, *J. Am. Chem. Soc.*, 2015, **137**, 7365–7370.
- 57 G. Baffou and R. Quidant, *Chem. Soc. Rev.*, 2014, **43**, 3898–3907.
- 58 Z. Xuming, C. Yu Lim, L. Ru-Shi and T. Din Ping, *Rep. Prog. Phys.*, 2013, **76**, 046401.
- 59 V. Subramanian, E. E. Wolf and P. V. Kamat, *J. Am. Chem. Soc.*, 2004, **126**, 4943–4950.
- 60 L. Xiaoguang, X. Di and Z. Zhenyu, *New J. Phys.*, 2013, **15**, 023011.
- 61 J. Sa, G. Tagliabue, P. Friedli, J. Szlachetko, M. H. Rittmann-Frank, F. G. Santomauro, C. J. Milne and H. Sigg, *Energy Environ. Sci.*, 2013, **6**, 3584–3588.
- 62 A. O. Govorov, H. Zhang and Y. K. Gun'ko, *J. Phys. Chem. C*, 2013, **117**, 16616–16631.
- 63 M. W. Knight, H. Sobhani, P. Nordlander and N. J. Halas, *Science*, 2011, **332**, 702–704.
- 64 K. Wu, J. Chen, J. R. McBride and T. Lian, *Science*, 2015, **349**, 632–635.
- 65 M. W. Knight, Y. Wang, A. S. Urban, A. Sobhani, B. Y. Zheng, P. Nordlander and N. J. Halas, *Nano Lett.*, 2013, **13**, 1687–1692.
- 66 L. Amidani, A. Naldoni, M. Malvestuto, M. Marelli, P. Glatzel, V. Dal Santo and F. Boscherini, *Angew. Chem., Int. Ed.*, 2015, **54**, 5413–5416.
- 67 Y. Tian and T. Tatsuma, *Chem. Commun.*, 2004, 1810–1811, DOI: 10.1039/B405061D.
- 68 T. Inagaki, K. Kagami and E. T. Arakawa, *Phys. Rev. B: Condens. Matter Mater. Phys.*, 1981, **24**, 3644–3646.
- 69 Y. Tian and T. Tatsuma, *J. Am. Chem. Soc.*, 2005, **127**, 7632–7637.
- 70 Y. Tian, X. Wang, D. Zhang, X. Shi and S. Wang, *J. Photochem. Photobiol., A*, 2008, **199**, 224–229.
- 71 Y. Tian, X. Shi, C. Lu, X. Wang and S. Wang, *Electrochem. Commun.*, 2009, **11**, 1603–1605.
- 72 J. E. Yourey, J. B. Kurtz and B. M. Bartlett, *J. Phys. Chem. C*, 2012, **116**, 3200–3205.
- 73 S. Cattarin, P. Guerriero, N. Dietz and H. J. Lewerenz, *Electrochim. Acta*, 1995, **40**, 1041–1049.
- 74 S. Mubeen, J. Lee, D. Liu, G. D. Stucky and M. Moskovits, *Nano Lett.*, 2015, **15**, 2132–2136.



- 75 H. M. Chen, C. K. Chen, Y.-C. Chang, C.-W. Tsai, R.-S. Liu, S.-F. Hu, W.-S. Chang and K.-H. Chen, *Angew. Chem., Int. Ed.*, 2010, **49**, 5966–5969.
- 76 H. Wang, G. Wang, Y. Ling, M. Lepert, C. Wang, J. Z. Zhang and Y. Li, *Nanoscale*, 2012, **4**, 1463–1466.
- 77 H. B. Yang, J. Miao, S.-F. Hung, F. Huo, H. M. Chen and B. Liu, *ACS Nano*, 2014, **8**, 10403–10413.
- 78 M. Bernardi, J. Mustafa, J. B. Neaton and S. G. Louie, *Nat. Commun.*, 2015, **6**, 7044.
- 79 A. M. Brown, R. Sundararaman, P. Narang, W. A. Goddard and H. A. Atwater, *ACS Nano*, 2016, **10**, 957–966.
- 80 A. Manjavacas, J. G. Liu, V. Kulkarni and P. Nordlander, *ACS Nano*, 2014, **8**, 7630–7638.
- 81 R. Sundararaman, P. Narang, A. S. Jermyn, W. A. Goddard and H. A. Atwater, *Nat. Commun.*, 2014, **5**, 5788.
- 82 S.-F. Hung, F.-X. Xiao, Y.-Y. Hsu, N.-T. Suen, H.-B. Yang, H. M. Chen and B. Liu, *Adv. Energy Mater.*, 2016, **6**, 1501339.
- 83 Y. Shiraishi, D. Tsukamoto, Y. Sugano, A. Shiro, S. Ichikawa, S. Tanaka and T. Hirai, *ACS Catal.*, 2012, **2**, 1984–1992.
- 84 A. Naldoni, F. Fabbri, M. Altomare, M. Marelli, R. Psaro, E. Selli, G. Salviati and V. Dal Santo, *Phys. Chem. Chem. Phys.*, 2015, **17**, 4864–4869.
- 85 F.-X. Xiao, S.-F. Hung, J. Miao, H.-Y. Wang, H. Yang and B. Liu, *Small*, 2015, **11**, 554–567.
- 86 F.-X. Xiao, Z. Zeng and B. Liu, *J. Am. Chem. Soc.*, 2015, **137**, 10735–10744.
- 87 H. Harutyunyan, A. B. F. Martinson, D. Rosenmann, L. K. Khorashad, L. V. Besteiro, A. O. Govorov and G. P. Wiederrecht, *Nat. Nanotechnol.*, 2015, **10**, 770–774.
- 88 A. Sousa-Castillo, M. Comesaña-Hermo, B. Rodríguez-González, M. Pérez-Lorenzo, Z. Wang, X.-T. Kong, A. O. Govorov and M. A. Correa-Duarte, *J. Phys. Chem. C*, 2016, **120**, 11690–11699.
- 89 W. R. Erwin, A. Coppola, H. F. Zarick, P. Arora, K. J. Miller and R. Bardhan, *Nanoscale*, 2014, **6**, 12626–12634.
- 90 H. Gao, C. Liu, H. E. Jeong and P. Yang, *ACS Nano*, 2012, **6**, 234–240.
- 91 P. Yuriy, T. Ivan, M. Kazuma, F. Nobuko, O. Ryoichi, T. Masahiro, S. Kiyoshi, G. V. Encarnacion and K. Takehiko, *Nanotechnology*, 2014, **25**, 315402.
- 92 X. Wang, K.-Q. Peng, Y. Hu, F.-Q. Zhang, B. Hu, L. Li, M. Wang, X.-M. Meng and S.-T. Lee, *Nano Lett.*, 2014, **14**, 18–23.
- 93 S. Nootchanat, H. Ninsonti, A. Baba, S. Ekgasit, C. Thammacharoen, K. Shinbo, K. Kato and F. Kaneko, *Phys. Chem. Chem. Phys.*, 2014, **16**, 24484–24492.
- 94 L. Enzhou, K. Limin, Y. Yuhao, S. Tao, H. Xiaoyun, Z. Changjun, L. Hanchen, W. Qiuping, L. Xinghua and F. Jun, *Nanotechnology*, 2014, **25**, 165401.
- 95 X. Zhang, J. Zhao, S. Wang, H. Dai and X. Sun, *Int. J. Hydrogen Energy*, 2014, **39**, 8238–8245.
- 96 H. J. Kim, S. H. Lee, A. A. Upadhye, I. Ro, M. I. Tejedor-Tejedor, M. A. Anderson, W. B. Kim and G. W. Huber, *ACS Nano*, 2014, **8**, 10756–10765.
- 97 P. S. Archana, N. Pachauri, Z. Shan, S. Pan and A. Gupta, *J. Phys. Chem. C*, 2015, **119**, 15506–15516.
- 98 D. Derkacs, S. H. Lim, P. Matheu, W. Mar and E. T. Yu, *Appl. Phys. Lett.*, 2006, **89**, 093103.
- 99 H. Dotan, K. Sivula, M. Gratzel, A. Rothschild and S. C. Warren, *Energy Environ. Sci.*, 2011, **4**, 958–964.
- 100 M. A. Green and S. Pillai, *Nat. Photonics*, 2012, **6**, 130–132.
- 101 L. Novotny and N. van Hulst, *Nat. Photonics*, 2011, **5**, 83–90.
- 102 J. A. Schuller, E. S. Barnard, W. Cai, Y. C. Jun, J. S. White and M. L. Brongersma, *Nat. Mater.*, 2010, **9**, 193–204.
- 103 D. M. Schaadt, B. Feng and E. T. Yu, *Appl. Phys. Lett.*, 2005, **86**, 063106.
- 104 I. Thomann, B. A. Pinaud, Z. Chen, B. M. Clemens, T. F. Jaramillo and M. L. Brongersma, *Nano Lett.*, 2011, **11**, 3440–3446.
- 105 A. Naldoni, F. Riboni, M. Marelli, F. Bossola, G. Ulisse, A. Di Carlo, I. Pis, S. Nappini, M. Malvestuto, M. V. Dozzi, R. Psaro, E. Selli and V. Dal Santo, *Catal. Sci. Technol.*, 2016, **6**, 3220–3229.
- 106 Y. Fang, Y. Jiao, K. Xiong, R. Ogier, Z.-J. Yang, S. Gao, A. B. Dahlin and M. Käll, *Nano Lett.*, 2015, **15**, 4059–4065.
- 107 H. Dotan, O. Kfir, E. Sharlin, O. Blank, M. Gross, I. Dumchin, G. Ankonina and A. Rothschild, *Nat. Mater.*, 2013, **12**, 158–164.
- 108 J. Li, S. K. Cushing, P. Zheng, F. Meng, D. Chu and N. Wu, *Nat. Commun.*, 2013, **4**, 2651.
- 109 F. F. Abdi, A. Dabirian, B. Dam and R. van de Krol, *Phys. Chem. Chem. Phys.*, 2014, **29**, 15272–15277.
- 110 A. Takai and P. V. Kamat, *ACS Nano*, 2011, **5**, 7369–7376.
- 111 N. Naseri, M. Qorbani, H. Kim, W. Choi and A. Z. Moshfegh, *J. Phys. Chem. C*, 2015, **119**, 1271–1279.
- 112 J. Wang, S. Pan, M. Chen and D. A. Dixon, *J. Phys. Chem. C*, 2013, **117**, 22060–22068.
- 113 W. Yuefan, K. Lin, K. Junhua, L. Hong, J. Zhihui, L. Xuehong, D. Hejun and S. Xiao Wei, *Nanotechnology*, 2012, **23**, 235401.
- 114 G. Liu, P. Li, G. Zhao, X. Wang, J. Kong, H. Liu, H. Zhang, K. Chang, X. Meng, T. Kako and J. Ye, *J. Am. Chem. Soc.*, 2016, **138**, 9128–9136.
- 115 R. van de Krol, in *Photoelectrochemical Hydrogen Production*, ed. R. van de Krol and M. Grätzel, Springer, US, Boston, MA, 2012, pp. 13–67, DOI: 10.1007/978-1-4614-1380-6\_2.
- 116 V. Subramanian, E. Wolf and P. V. Kamat, *J. Phys. Chem. B*, 2001, **105**, 11439–11446.

